Univerzita Karlova
Přírodovědecká fakulta

Studijní program: Geotechnologie
Studijní obor: B-GEOTEC

Alevtina Kuznetsova

Geological and gravimetric pattern of Ethiopia

Geologický a tíhový obraz Etiopie

Bakalářská práce

Vedoucí práce:

Mgr. Jan Valenta, Ph.D.

Konzultanti:

Dipl.-Ing. Christiane Malá

doc. RNDr. Kryštof Verner, Ph.D.

Prague, 2024

Charles University
Faculty of Science

Study programme: Geotechnology
Branch of study: B-GEOTEC

Alevtina Kuznetsova

Geological and gravimetric pattern of Ethiopia

Geologický a tíhový obraz Etiopie

Bachelor´s thesis

Supervisor:
Mgr. Jan Valenta, Ph.D.
Consultants:
Dipl.-Ing. Christiane Malá
doc. RNDr. Kryštof Verner, Ph.D.

Prague, 2024

Prohlášení:

Prohlašuji, že jsem závěrečnou práci zpracovala samostatně a že jsem uvedla všechny použité informační zdroje a literaturu. Tato práce ani její podstatná část nebyla předložena k získání jiného nebo stejného akademického titulu.

V Praze 11.12.2023

Podpis

Contents

Abstrakt

Etiopie je z geologického hlediska unikátní zemí, kde lze studovat projevy aktivní tektoniky v kontextu rozsáhlého vývoje východoafrického riftového systému (East African Rift System – EARS), jehož součástí je i hlavní etiopský rift (Main Ethiopian Rift – MER). Hlavní etiopský rift (MER) je typickým kontinentálním riftem, který se rozprostírá se mezi africkou, somálskou a arabskou litosférickou deskou, a to v linii přes 6000 kilometrů od Sýrie po centrální Mosambik.

Studie tíhového pole ukazuje na významné ztenčení zemské kůry v oblastech hlavního etiopského riftu a severní části Afaru, tato kůra má převážně charakter kůry oceánské. V jižní část Afaru má zemská kůra mocnost mírně vyšší, a navíc pravděpodobně obsahuje významný podíl kontinentální kůry. Pochopení procesu ztenčování zemské kůry v kontextu aktivního riftingu je zásadní pro předpovídání budoucích geodynamických událostí v tomto regionu, což je klíčové pro udržitelný život rychle rostoucí populace a výstavbu nezbytné infrastruktury.

Tato práce analyzuje archivní tíhová data shromážděná z měření na zemského povrchu i data získaná leteckým měřením (archiv etiopské geologické služby) ve spojení s dostupnými geologickými a strukturními daty za účelem vyhodnocení celkového tíhového účinku v oblasti Etiopie a určení hlavních geologických struktur ve dvou oblastech jižní části MER – v zónách Gedeo a Sidama. Soubory tíhových dat byly zpracovány v softwarech ArcGis a Surfer za účelem vytvoření Bouguerových map tíhových anomálií.

Mapa úplných Bouguerových anomálií (Complete Bouguer Anomalies – CBA) celého etiopského území odhaluje kontrastní oblasti s projevy tíhových maxim a minim, včetně struktury hlavního etiopského riftu (lokální tíhová maxima v důsledku ztenčování kůry). Západní i východní plató vykazuje tíhové minimum. Pro oblast Afaru je charakteristická mírně pozitivní tíhová anomálie, zatímco jižní část etiopského riftu a rift Turkana vykazují negativní gravitační anomálie. Nárůst hodnot CBA dokládá odhady, že tloušťka kůry klesá směrem k severu, a to od hodnot cca. 50 km v oblastech vyzdviženého plató, na hodnoty cca. 20 km v oblasti Afaru, kde je také předpokládána významnější přítomnost oceánské kůry s vyšší hustotou.

Mapy úplných Bouguerových anomálií pozemních i leteckých tíhových dat ukazují podobné změny tíhového pole v zóně Gedeo a oblasti Sidama, a to s mírnými rozdíly na jihu a jihovýchodě. Hlavní geologické a tektonické rysy zóny Gedeo a regionu Sidama jsou porovnávány s nově vypočtenými Linsserovými indikacemi. Výsledky jsou v dobré shodě s předchozími výzkumy a dále je dopňují, především v odahu rozsahu prekambrického krystalinika pod vrstvami riftového vulkanismu.

Klíčová slova: geologie, gravimetrie, Etiopie, etiopský rift

Abstract

From a geological point of view, Ethiopia is a unique country where active tectonics displays can be studied, in the context of extensive East African Rift System (EARS) evolution, where the Main Ethiopian Rift (MER) is a part. The Main Ethiopian Rift (MER) is typical continental rift structure spread between the African, Somali, and Arabian lithospheric plates stretching over 6,000 kilometres from Syria to central Mozambique.

This study of the gravity pattern in Ethiopia reveals significant crustal thinning in the Main Ethiopian Rift and Northern Afar regions. In the southern Afar, the earth's crust has a slightly higher thickness and, moreover, probably contains a significant proportion of the continental crust. The understanding of crustal thinning in the context of active rifting is essential to predict future geodynamic events in that region, which is crucial for the sustainable life of a rapidly expanding population and the necessary construction of infrastructure.

This work provides an analysis and re-interpretation of archival gravity data collected from land surface surveys and airborne gravity studies (archive of Geological Survey of Ethiopia) in conjunction with available geological and structural data to evaluate overall gravimetric pattern of Ethiopia and determine main geological structures in two key areas of the southern MER – in Gedeo and Sidama Regions. The gravity datasets were processed in ArcGis and Surfer softwares to create Bouguer gravity anomaly maps.

The Complete Bouguer Anomalies (CBA) map of the entire Ethiopian territory reveals contrasting regions with manifestations of gravity maxima and minima, including MER (local gravity maxima due to crustal thinning). The western plateau shows a low gravity pattern, and the eastern plateau reveals a negative anomaly. The Afar triple junction shows slightly positive anomalies in line with the Ethiopian rift, while the southern Ethiopian rift and the Turkana rift have negative gravity anomalies. The increase in CBA values estimates that crustal thickness decreases northward from about 50 km in the non-rifted areas to about 20 km in the Afar region where a more significant presence of higher-density oceanic crust is also assumed.

Maps of the Complete Bouguer Anomalies of the land and airborne gravity datasets demonstrate similar gravity anomaly variations in the Gedeo Zone and Sidama Region with a slight difference in the south and southeast. The main geological and tectonic features of the Gedeo Zone and Sidama Region are compared with newly calculated Linsser's indications. The results are in strong agreement with previous research done for the Ethiopian region in terms of different origin of geological structure, orientation, and nature.

Key words: geology, gravity, Ethiopia, Main Ethiopian Rift

Acknowledgement

This Bachelor Thesis was processed in frame of the Czech development cooperation project in Ethiopia entitled ""“Ensuring Sustainable Land Management in Selected Areas of Ethiopia on the Basis of Geoscientific Mapping” in the years 2021 to 2023.

I would like to thank my supervisor, Mgr. Jan Valenta, Ph.D for his guidance and valuable suggestions during the process of writing my thesis. I learned a lot from his serious scientific approach and deep knowledge of geophysics. I am grateful to my consultant doc. RNDr. Kryštof Verner, Ph.D. for all his reccomendations, but most importantly – for inspiriting me to be an adventurer and increase my knowledge about the world every day, he is a great inspiration for many budding scientists. Also, I express my deep gratitude to Dipl.-Ing. Christiane Malá from ČVUT for enormous help and guiding my work constantly, your explanation about structure of the work and scientific research were crucial for me and I will always be grateful for such care and support you provided me during such difficult times. Furthermore, I would like to thank my family and my ‘philosophical father’ Niall Lambkin, your philosophical lessons taught me to see light in the deepest darkness and be able to withstand life no matter how unbearable it can be.

To all of them and many others, my sincere thanks and gratitude

1. Introduction

Ethiopia is an unique land from a geological perspective, it is located in the Horn of Africa, where an active continental rifting can be observed (Chorowicz, 2005). Analysis of the exact geo-tectonic events in this region helps not only to determine the geological past but also contribute to reliable predictions of the future for the whole region. Gravity survey plays a crucial role in analysis of tectonic structures, overall geological pattern, can predict tectonic and seismic activity (Tiberi et al., 2005).

In the context of modern survey technologies including e.g., land-surface, airborne and satellite measurements, the today's possibilities to generate large gravity datasets of regions of interest is better than ever before. With the help of computational technology and highly developed data processing technologies these huge collections of gravity data can be evaluated in high details. The processed data can then be used to create regional gravity anomaly maps which can be further analyzed and compared. The origin of these gravity anomalies is the result of interaction of the geological pattern and the activity of the current regional stress-field in the earth's crust.

The gravity field of Ethiopia shows that the Main Ethiopian Rift and northern Afar have regional gravity minimums indicating distinct crustal thinning due to continental rifting. The gravity field of the Main Ethiopian Rift (MER) suggests that the crust beneath the central MER is thicker compared to the southern Afar region**.** This difference in crustal thickness is attributed to the presence of higher density lower crust within the southern Afar region, which is likely composed of mafic material. This higher density lower crust could be associated with the increased extension observed in the region (Rogers, 2006).

Sidama region and the Gedeo zone (Figure 5 and 6) were selected for this study in order to determine the detailed geological structure of the Central Main Ethiopian Rift (CMER) and Southern Main Ethiopian Rift (SMER). Both areas have undergone varying stages of continental extension (rifting) between the Nubian and Somalian plates, which resulted in formation of typical rift-related topography including escarpments, horsts, grabens, and highly elevated plateau along principal rift structure (Buriánek et al., 2022; Verner et al., 2022).

This research work shall contribute to the understanding of gravity field variations in Ethiopian region, with a special focus to Gedeo Zone and Sidama Region. Combining a theoretical and a practical part, it gives an

extensive overview about the most recent geological and tectonic evolution which also includes new generated results of gravity anomaly mapping of Ethiopia. The geological part provides an overview of Ethiopia's geological evolution, traversing through its geological formations and significant geological events based on a summary of existing literature (Bonini et al., 2005; Corti, 2009; Fritz et al., 2013; Gani et al., 2009; Thiessen et al., 1979). The summary of geological settings is followed by an explanation of the methodology used in gravimetry survey (Hinze et al., 2012; Mickus and Hinojosa, 2001; Tang et al., 2019; Virtanen, 2006; Zhang et al., 2000) including the application of the Linsser Indications Technique (Linsser, 1967; Murata Y. and Noro H., 1994; Nettleton, 1971; Sefara, 1973; Wybraniec, 1999).

The main goal of this work is to unveil fault systems in CMER and SMER, especially in Gedeo Zone and Sidama Region, where a Czech Development Cooperation Project is currently working on compilation of a geological and hydrogeological map with practical implications of sustainable management of soil and water resources (Verner et al. 2022).

2. Geological Settings

The geology of Ethiopia can be broadly divided into three main geological units, each representing distinct rock formations and geological processes. These units are (Tefera et al., 1996):

(a) The Precambrian units. These rocks are typically metamorphic in nature due to the intense pressure and temperature associated with the process of subduction and continental collision in frame of the East-African Orogeny, which was associated with the formation of the Gondwana Continent. The Precambrian units form the "basement" of rock environment in Ethiopia which is classified as the Hammar Domain within the Arabian-Nubian Shield (ANS) cropping out in erosional relicts, in form of four shields (-northern, -southern, -western and -eastern). After the East African orogenic event, the Precambrian orogenic mountain ranges underwent extensive peneplanation and were nearly entirely eroded during the Paleozoic (Davidson 1983; Gani et al. 2007).

In Ethiopia, 23% of the landmass is comprised of Precambrian metamorphic and intrusive igneous rocks. The high-grade gneisses and migmatites, known as the Lower Complex, are part of the Mozambique Orogenic Belt and consist mainly of amphibolites and orthogneisses, with occasional granulite facies and bands of marble. Conversely, the Upper Complex, which consists of related mafic to felsic intrusives and low-grade volcano-sedimentary rocks, is part of the Pan-African Arabian-Nubian Shield. The contacts between the high-grade and low-grade rock units are typically marked by the linear belts of mafic and ultramafic rocks, which are frequently found along major shear zones. The ages of these rocks typically range between 900 and 500 million years, except for some older Archean and Mesoproterozoic ages found in certain units (Tadesse et al., 2003).

(b) Paleozoic-Mesozoic sedimentary units. These rocks crop out in form of large sedimentary basins which have the significant geological and economic importance (Gani et al., 2009). Three distinct sedimentary basins, namely the Ogaden Basin (350,000 km2), the Abay (Blue Nile) Basin (63,000 km2), and the Mekele Basin (8,000 km2), cover 25% of Ethiopia's landmass. The formation of these

basins can be attributed to the multiple stages of the Gondwanaland breakup, which involved reactivation along preexisting Precambrian structures. Rifting associated with the breakup of Gondwanaland, particularly from the late Carboniferous period onwards, led to the development of these basins within the continental African plate and along its margins. (Tadesse et al., 2003)

(c) Cenozoic volcanic rocks and associated sediments. The central part of Ethiopia from north to south is marked by the presence of the East African Rift System (EARS) which is prominent rift structure as the result of continental extension between the African, Nubian, and Somali plates. This area is characterized by active faulting and volcanic activity that has contributed to the formation of steep escarpments, grabens, and volcanic phenomena. Surrounding Ethiopian Plateau is a vast highland characterized by extensive plateau and mountain ranges, including the Ethiopian Highlands, which rise to heights exceeding 4,000 meters. The plateau consists of volcanic rocks of Cenozoic age (Bonini et al., 2005).

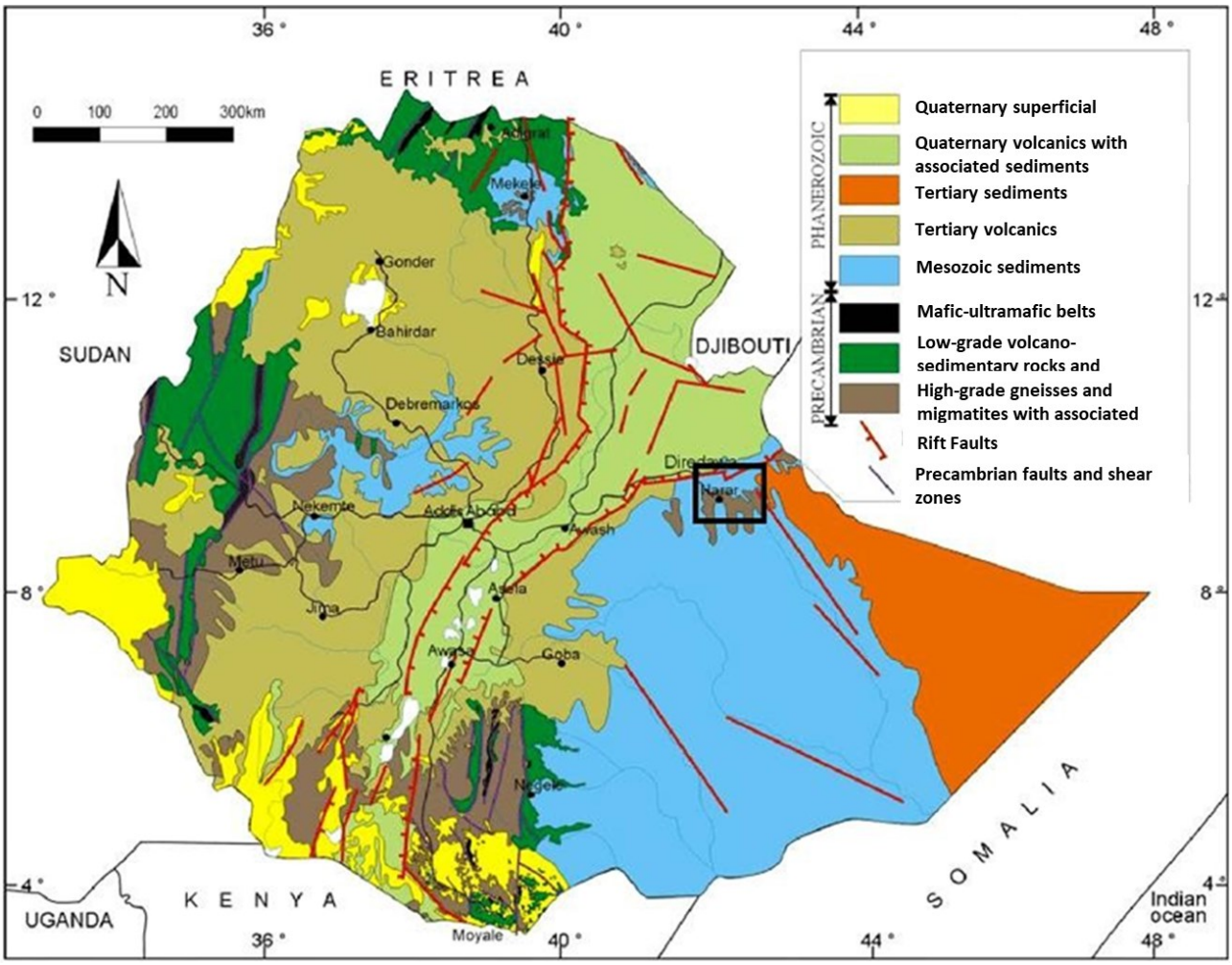

Figure 1. Simplified sketch of geological map of Ethiopia (modified after Tefera et al. 1996).

2.1 East African Rift System (EARS)

The EARS (Figure 2) is active rift system driven by pulling apart the African, Arabian, and Somalian litho-spheric plates. Due to the rifting the highly uplifted plateau surrounding the rift zones were formed. These plateau are associated with upwelling hotspots that have been active since the Eocene-Oligocene era (Corti, 2009).

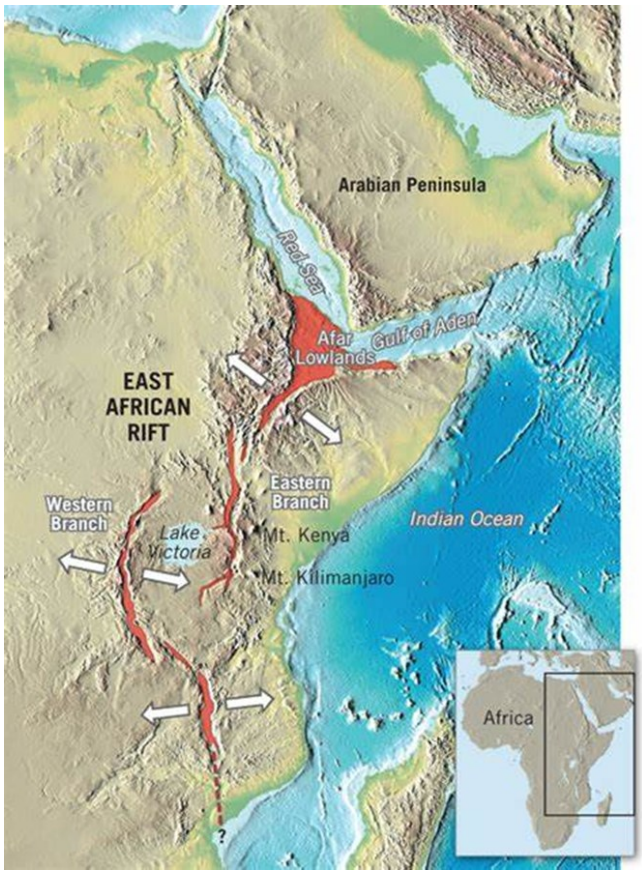

Figure 2: The digital elevation model illustrates northeast-ern Africa highlighting the presence of the East African Rift System, Afar Depression, Red Sea Rift, Gulf of Aden Rift (Wright et al., 2016)

The EARS spans the uplifted regions of Ethiopia and Kenya and is associated with the Ethio-Afar and Kenyan hotspots (Thiessen et al., 1979). The Main Ethiopian Rift (MER) in Ethiopia exhibits a distinct northeast-southwest extension zone and volcanically active structures (Rogers, 2006). South of Turkana, the EARS divides into the Eastern Rift and Western Rift. The Eastern Rift extends southward to Tanzania, characterized by extensive mafic lava eruptions. This East African Rift System was probably initiated from early Miocene, but there is also evidence for earlier Paleogene rift activity, mainly in northern Kenya and Ethiopia (Corti, 2009; Ebinger et al., 1993; Hendrie et al., 1994). The Western Rift, with notable mountain ranges and limited magmatism, stretches from western Uganda to northern Mozambique. The western rift has been initiated later than the eastern rift, during the late Miocene (Ebinger et al., 1989). These rifts converge at the Turkana Depression, forming the EARS. Both rift systems are tectonically active nowadays.

2.2 Afar Depression

The Afar Depression is active continental rifting plate boundary located between Somalian, Arabian and Nubian plate. It spans an area of about 250,000 square kilometers and is surrounded by steep fault escarps and marginal grabens (Beyene and Abdelsalam, 2005; Collet et al., 2000).The depression is bordered by the Ethiopian escarpment to the west, the Danakil Microplate to the east and northeast, and the Somalian Plateau to the south. The elevation ranges from over 3500 meters above sea level on the Ethiopian plateau to approximately 146 meters below sea level in the northern Afar Depression (Dallol Depression) (Tesfaye et al., 2003). The Afar Depression is divided into northern, central, and southern sectors based on its physiography and tectonic divisions.

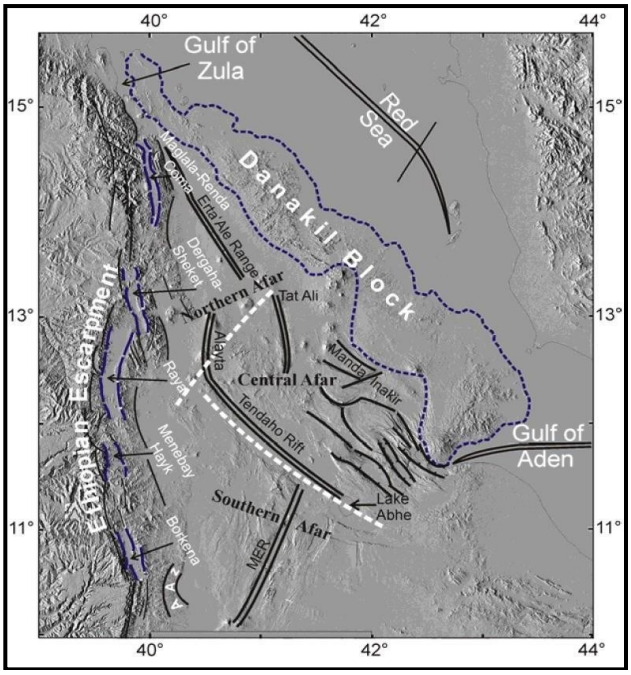

Figure 3: Afar Depression and its surrounding areas, including plateau, are depicted (Tesfaye et al., 2003). Tectonic zones and marginal basins within the depression are indicated by dashed lines (white and blue, respectively). The white dashed lines divide the Afar Depression into northern, central, and southern sections. Active spreading ridge segments of the Afar Depression, Red Sea, and Gulf of Aden are represented by double black lines. AAZ refers to the arcuate accommodation zone.

The northern Afar Depression (the Danakil Depression) is a subsided area bordered by the Ethiopian highlands on the west and the Danakil Block on the east. It has an average elevation of around 200 meters and features the Erta'Ale Range, a volcanic range running in NNW-SSE direction. The deepest part of the depression is called Dallol, where the elevation drops to approximately 146 meters below sea level. The volcanic structures in the depression align parallel to the regional tectonic trend of the Red Sea rift add (Tesfaye et al., 2003). The depression contains lacustrine sediments, evaporite beds, and basaltic lava flows. Sedimentation in the northern Afar Depression began in the Oligocene- Miocene period and

continued with Piedmont sediments and shallow water carbonates in the Pliocene-Recent (Barrat et al., 1998). The depression became arid after being separated from the Red Sea by the Alid volcanic center.

The central Afar Depression features grabens, horsts, and volcanic shields, and it hosts the world's only active sub-aerial triple junction. The Tendaho rift, a significant structure in this region, marks its south-western boundary. The Tendaho rift displays prominent fault scarps witha maximum displacement of about 100 meters, creating steep topographic gradients (Acocella, 2010). The region is characterized by parallel sets of northwest-oriented grabens and horsts, resulting in an average elevation of around 450 meters (Tesfaye et al., 2003).

The southern Afar Depression, an extension of the MER, exhibits horst andgraben features similar to the central Afar (Beyene and Abdelsalam, 2005). However, it is characterized by NNE-trending right-stepping horsts and grabens. The mean elevation of the southern Afar Depression is approximately 700 meters, gradually decreasing towards the Tendaho graben. The central part of the southern Afar contains dis-continuous grabens arranged in an en-echelon pattern, associated with the northward extension of the active extensional rift zone called the Wonji Fault Belt (WFB) of the MER.

The marginal grabens, located at the base of the escarpment, formed during the middle Oligo- Miocene period through transtensional faulting. The western margin of the Afar Depression exhibits reactivated deformational features, including down-warping, faulting, and tilting of blocks due to magma injection blocks (Zanettin and Justin-Visentin, 1975). The eastern boundary is marked by the Somalian escarpment, characterized by a network of closely spaced normal fault.

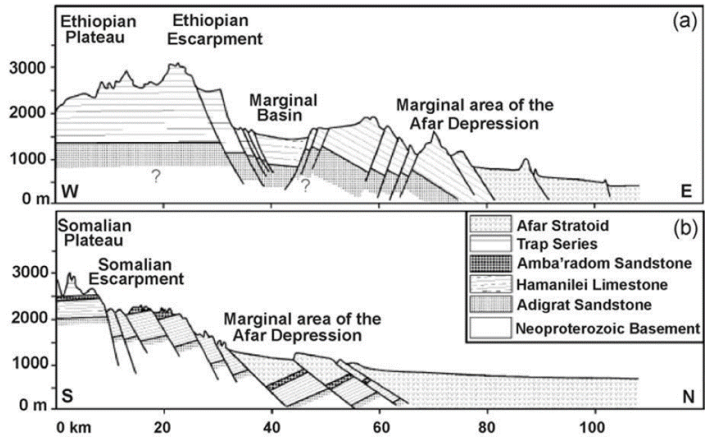

Figure 4: The geological cross-sections illustrate crustal deformation along the Ethiopian and Somalian margins of Afar. (a) Marginal basins are bounded by antithetic and synthetic faults. (b) The southern/Somalian margin is characterized by book-shelf type faulting and dominant half-grabens (Beyene and Abdelsalam, 2005).

2.3. Main Ethiopian Rift (MER)

The Main Ethiopian Rift (MER) is the northernmost part of the EARS, connecting with the Red Sea and Gulf of Aden rifts. It consists of two main segments: the Afar Depression and the Main Ethiopian Rift (Corti, 2009). The MER is a narrow rift valley separating the Nubian and Somalian plates, widening as it extends into the Afar Depression. This region is known as an arcuate accommodation zone and marks the southern boundary of the Red Sea propagator. The Main Ethiopian Rift is the northernmost segment of the EARS and connects it with the Afar Depression. The MER extends from the southern Afar Depression to the northern end of the Turkana Depression. It formed through the southward propagation of the Red Sea rift and the northward migration of the EARS (Tommasini et al., 2005). Over time, the MER deepened and widened, developing through a series of overlapping half-graben segments.

The earliest volcanic activity of SMER corresponds to the initiation of flood basalt volcanism during the Paleogene period (Corti, 2009) transitional tholeiitic flood basalts (Ebinger et al., 1993). The second episode of volcanism occurred from 18 to 11 Ma (Ebinger et al., 1993) attributed to ascent of mantle plume (George and Rogers, 2002). Subsequently, rifting ensued in the broadly rifted zone during the Miocene (Boone et al., 2019; Philippon et al., 2014). Following Pleistocene to Holocene late-rift volcanic activity ensued along with volcaniclastic rocks and pyroclastic deposits (Ebinger et al., 1993). The late-rift (Pleistocene) volcanic activity in the southern Main Ethiopian Rift is dominated by the sequence of acid volcaniclastic deposits, alkali basalt to trachyte lava flows, and pyroclastic cones (Ebinger et al., 1993) The most recent deposits are those of Holocene age lacustrine sediments related to fluctuations of Lake Awassa (Minissale et al., 2017).

2.4 Geology of Sidama Region and Gedeo Zone

The SMER encompasses the Gedeo Zone and Sidama Region (Figure 5 and 6), covering 1,347 and 6,538 square kilometers, respectively. The Gedeo and Sidama Zones lie along the eastern border of the SMER, which extends in a NNE–SSW direction as a part of the broader East African Rift System (Bonini et al., 2005; Ebinger et al., 2000).

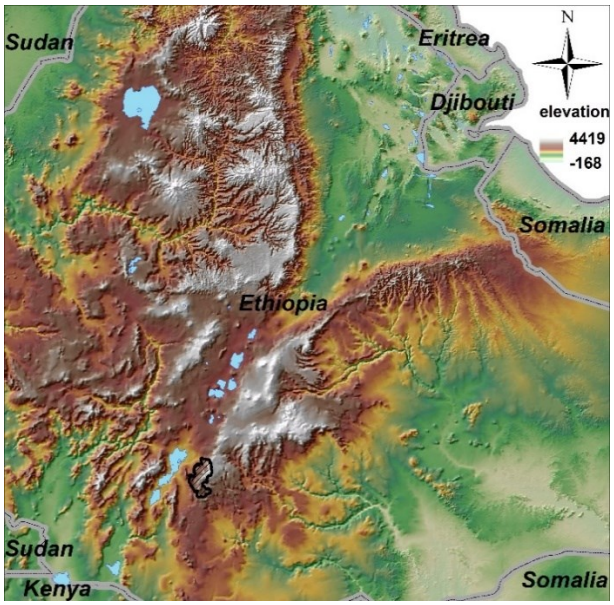

Figure 5: Schematic DMR map and location of the Gedeo Zone (southern Ethiopia).

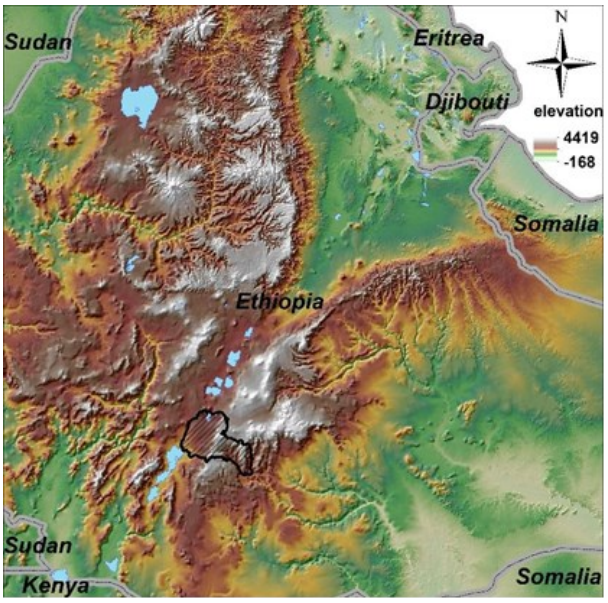

Figure 6: Schematic DMR map and location of the Sidama Region (southern Ethiopia).

From the geological point of view the high to medium grade metamorphic rocks of the Neoproterozoic southern Ethiopian Shield exposed in deeply eroded valleys are overlaid by rift-related volcanic and volcanoclastic formations spanning from Eocene to recent times. The metamorphic rocks belonging to the Adola-Moyale Belt and the Akobo, Surma, and Hammar domains exhibit different metamorphic grades and are interspersed with ophiolitic-volcano sedimentary units such as Kenticha, Megado, and Bulbul (Ghebreab, 1992; Verner et al., 2021; Worku, 1996; Yibas et al., 2002; Yihunie et al., 2004).

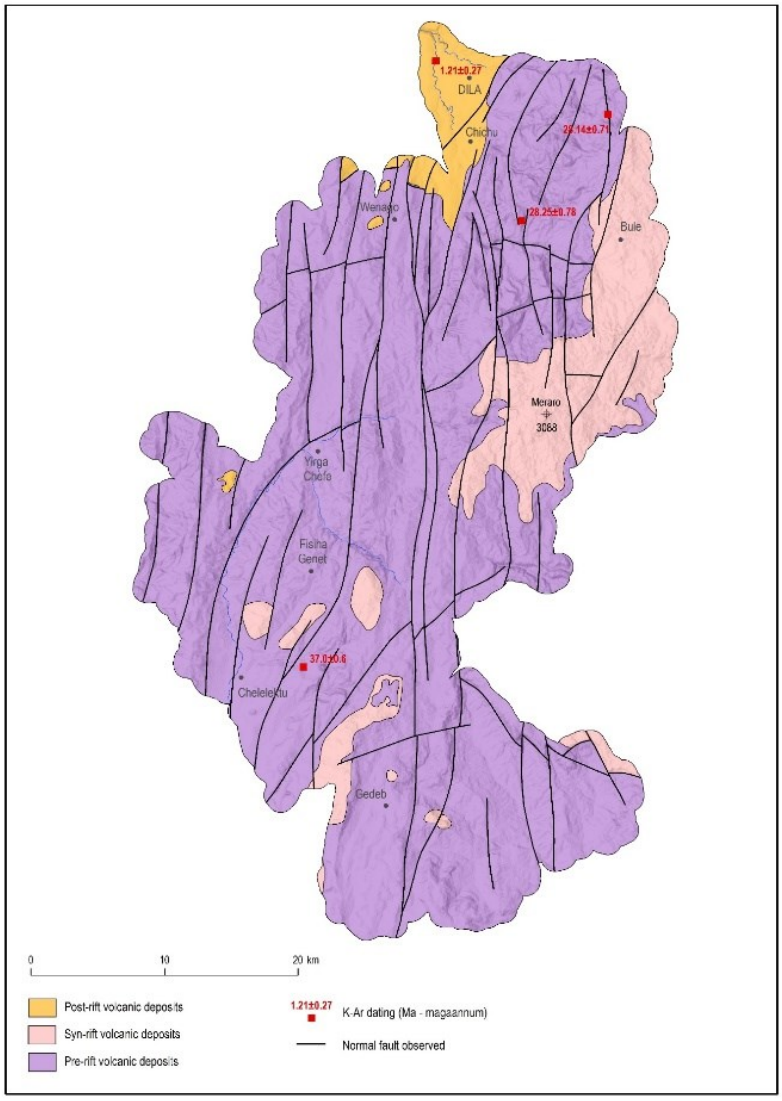

Figure 7: Schematic geological map of the Gedeo Zone (Buriánek et al 2022)

The rift-related volcanic rocks range in age from the Paleogene to Neogene periods, separated by faults that emerged from the Miocene to the present, creating horsts and grabens structures (Ebinger et al., 2000; Ebinger and Casey, 2001). Frequent tectonic activity, linked to the southwestward migration of the Main Ethiopian Rift, has notably impacted the southern rift section during the Pliocene to Pleistocene period. Different segments of the MER represent various stages of a regional continental extension. This extension began with early rifting in the SMER during the Lower Miocene period and later intensified in the central and northern sections (Corti in 2009). Over time, the original ~WNW–ESE extension direction has evolved into the current ~W(WSW)–E(ENE) orientation. Evidence of the reactivation of previous normal faults, resulting in shifts in the regional stress field orientation from perpendicular extension to ~WSW–ESE transtension, has been observed in multiple areas across the MER (Agostini et al., 2011).

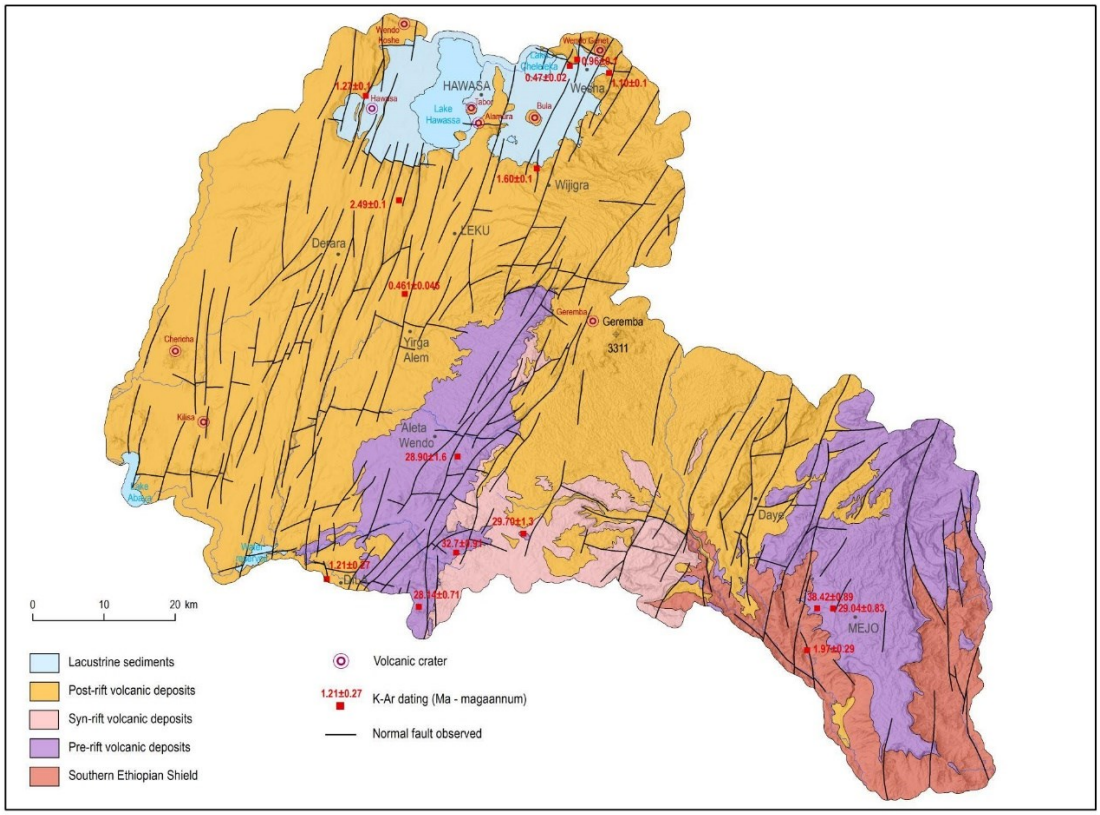

Figure 8: Regional geological schematic map of the Sidama Region (Verner et al 2022)

The area of Gedeo Zone and Sidama Region is composed of three distinct lithotectonic units formed within the context of the SMER (Verner et al. 2022; Buriánek et al. 2022): (a) Pre-rift effusive rocks and volcanic-clastic deposits dating from the Eocene to Oligocene periods. This sequence includes a variety of rocks with different compositions, such as the Amaro–Gamo basalts, interspersed with ignimbrites and related acid pyroclastic deposits. (b) Early-rift volcanic deposits, primarily consisting of basalt lava flows along with lesser amounts of welded rhyolitic ignimbrites and rhyolite lava domes. These deposits also contain subordinate volcanic breccias and span the Miocene to Pliocene ages. (c) Late-rift rift-floor volcanic deposits of Pleistocene age, characterized mainly by sequences of rhyolitic to trachytic ignimbrites accompanied by pyroclastic fall deposits. These deposits are collectively referred to as the Dino Formation. The regional tectonic pattern reflects different stages of geological evolution with the oldest ductile to brittle deformation associated with the metamorphic basement units. The subsequent tectonic manifestations of faults forming different population of attitude are characterized as NE-SW directed earlier extension followed by recent extensions in the ENE-WSW direction (Verner et al. 2022).

3. The Methodology of Gravimetry

Gravimetry is a non-invasive geophysical method which detects the strength of Earth's gravitational field and its difference at specific points for further evaluation of geological structures. Gravity method is widely used in engineering, hydrogeology, and geological exploration, mainly for identification of karsts, prediction of bedrock structure and upper layer thickness, monitoring geothermal and groundwater reservoir conditions (Saibi, 2018). Gravimetry is also have an important role in hydrocarbon (Gadirov et al., 2022; Zhang et al., 2019), geothermal (Mulugeta et al., 2021; Saibi et al., 2012) and mineral exploration (Tanner and Gibb, 1979; Zhang et al., 2020).

Gravity measurements primarily rely on variations in subsurface material density. Several numerical and analytical methods are available to study and interpret these gravity variations in terms of geometry, depth, and density of the sources. These methods include Fourier transformation, Euler deconvolution, Mellin transform, least-squares minimization approaches and neural network (Mickus et al., 2007).

It is important to associate GPS measurements with gravity data to determine precise coordinates (longitude and latitude) and, especially, altitudes of gravity stations. Processed gravity data, known as Bouguer gravity, is obtained by removing quantifiable disturbances and is typically measured in milligals (mGal). Advanced computer models can now generate three-dimensional density models of the subsurface based on gravity data interpretation (Murray, 1997).

Newton's law of gravity $F = G\frac{m_1 m_2}{r^2}$ is the foundation of the gravimetry method which illustrates the dependence of the gravitational force F on masses m_1 and m_2 and their distance. The following form of Newton's law is used for calculation of gravitational acceleration:

$$g = G\frac{M_E}{R_E^2} \qquad (1)$$

Where:

M_E is the mass of the Earth = 5,974·10^{24} kg

G is the universal gravitational constant = 6.674 ·10^{-11} N·m^2/kg^2

R_E^2 is the radius of the Earth (Mareš, 1990)

The *g* value obtained from the above equation will have units in SI system as m/s^2 (and Gals for interpreting gravitational data in scientific circle). The average earth's gravitational acceleration is 980 Gals (Lowrie and Fichtner, 2020) at the earth's surface. Mostly in gravity survey the acceleration of gravity variations is in the range of 10^{-1} to 10^{-3} Gals, therefore mostly the units milliGal (mGal) is used in gravity data interpretation and in engineering and environmental studies even the smaller units of microGal (μGal) are used (S. Essa and E. Diab, 2022).

As the gravimetry is related to the subsurface discrepancies with respect to mass dispersals, therefore most gravity data interpretation method uses the above-mentioned gravity acceleration equation. By using the integral equation this task can be achieved by resolving the gravitational field resulting from a mass distribution. In most of the gravity methods, typically vertical (z) component of g is measured by the gravity meter, though using the three components of gravity field can enhance the effectiveness of utilizing the gravity gradient tensor in exploration tasks, as highlighted by Mickus and Hinojosa in 2001.

A density anomaly in gravity method is defined as deviation of corrected gravity values that could be produced by the subsurface layers of uniform thickness. To have a gravity anomaly that could be measured, there must be (1) a contrast in density between the geological structures and adjacent rock formations (2) a favorable correlation exists between the position of gravity station locations and geometric characteristics, including depth, of the geological feature of interest.

3.1 Densities of Rocks

In surface gravity exploration, we look for lateral density contrasts that we can relate to subsurface geologic features, such as stratigraphic changes, faults, and folds. A geological layer which does not have any structural or stratigraphic changes will not show gravity anomalies, because there is no lateral density contrast present. In this section, we look at rock densities and practical methods for determining them. The bulk density of a rock is calculated by adding together the volume fraction of each constituent minerals multiplied by its respective density ρ.

Local gravity anomalies are caused by lateral density contrasts. If horizontal density layering is uniform, then we will observe no local gravity anomalies. Once we have selected a base density, we can compute density contrasts as follows:

$$\Delta\rho = \rho a - \rho b \qquad (2)$$

Where Δρ is the density contrast, ρ_a is the anomalous density and ρ_b is the background density (Mareš, 1990)

For example, if a sufficient sulfide ore body with a bulk density of 4.0 g/cm^3 is located in a limestone with a density of 2.7 g/cm^3, the density contrast of the ore body will be +1.3 g/cm^3. The amplitude of the gravity anomaly observed from such an ore body is proportional to the density contrast (Alden, 2020).

Table 1. Densities of minerals and rocks (Alden, 2020)

Mineral	**Density (g/cm^3)**	**Rock**	**Density (g/cm^3)**
Apatite	3.1–3.2	Andesite	2.5–2.8
Biotite Mica	2.8–3.4	Basalt	2.8–3.0
Calcite	2.71	Coal	1.1–1.4
Chlorite	2.6–3.3	Diabase	2.6–3.0
Copper	8.9	Diorite	2.8–3.0
Feldspar	2.55–2.76	Dolomite	2.8–2.9
Fluorite	3.18	Gabbro	2.7–3.3
Garnet	3.5–4.3	Gneiss	2.6–2.9
Gold	19.32	Granite	2.6–2.7
Graphite	2.23	Gypsum	2.3–2.8
Gypsum	2.3–2.4	Limestone	2.3–2.7
Halite	2.16	Marble	2.4–2.7
Hematite	5.26	Mica schist	2.5–2.9
Hornblende	2.9–3.4	Peridotite	3.1–3.4
Iridium	22.42	Quartzite	2.6–2.8
Kaolinite	2.6	Rhyolite	2.4–2.6
Magnetite	5.18	Rock salt	2.5–2.6
Olivine	3.27–4.27	Sandstone	2.2–2.8
Pyrite	5.02	Shale	2.4–2.8
Quartz	2.65	Slate	2.7–2.8
Sphalerite	3.9–4.1		
Talc	2.7–2.8		
Tourmaline	3.02–3.2		

3.2 Gravity data acquisition

The process of gravity data acquisition involves the measurement of gravitational force acting on a test mass within the instrument. This is achieved by using methods like free-fall, pendulums, measuring downward force with a spring, or by using an electromagnetic accelerometer. In earth studies the demand of high accuracy and spatial resolution for gravity measurements which require a careful selection of survey instruments, design, and data acquisition parameters (Hinze et al., 2012).

In geological studies, gravity measurement accuracy is within the range 1 to 0.01 mGal is necessary, while investigations of shallow zones and monitoring time variations the accuracies are in the range of 0.001 mGal or 1 μGal.

Spatial resolution is also very important, determining the minimum separation needed to distinguish individual adjacent sources and identify small features in a survey. Resolution is typically expressed as the minimum half-wavelength that can be effectively mapped, considering the accuracy limits of the observations and reductions (Hinze et al., 2012). On land, resolution depends on the data interval, adjusted based on survey objectives. Moving platforms like marine vessels, aircraft, and satellites use virtual intervals established through filtering consecutive observations to remove motion-related noise. Accuracy and spatial resolution have a non-linear relationship, with decreasing accuracy as resolution or the minimum observable wavelength decreases. Hence, achieving the required accuracy and resolution is crucial to avoid limitations in data acquisition determining study objectives.

Accuracy and spatial resolution in dynamic survey systems are complex (Figure 9). Fairhead and Odegard 2002, compared gravity accuracy and resolution over time, showing improvements due to the use of lighter-than-air airships for airborne gradiometric surveys, which provide stability and relatively low speed (Hatch, 2007; Hatch and Pitts, 2010).

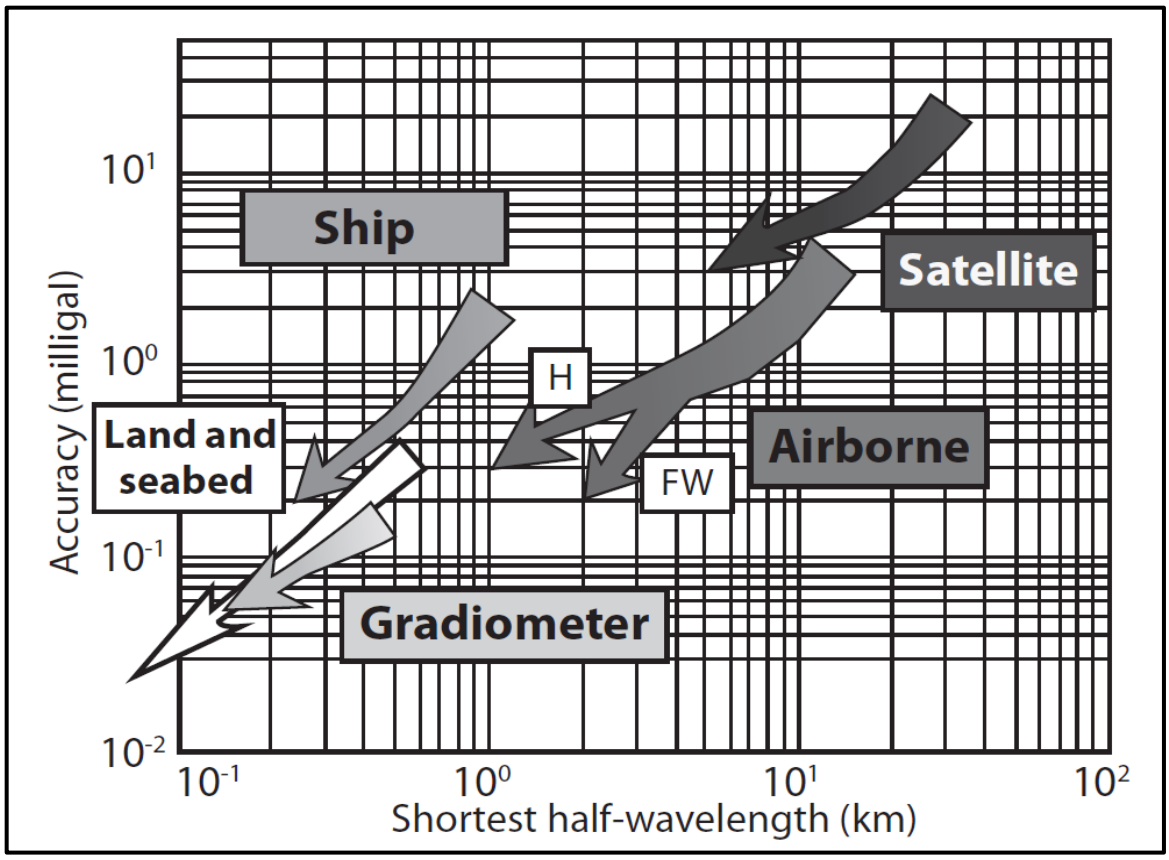

Figure 9: The relative accuracies and wavelength resolutions of various gravity surveying methodologies are depicted in a log-log time-trend plot, indicating the inferred optimal gravity resolutions of different survey systems. The arrow points on the plot represents the current claims. The abbreviations used in the plot include FW for fixed-wing aircraft and H for helicopter aircraft. In addition, drillhole gravimeters have an accuracy of a few microgals and a resolution of approximately 10m, and absolute gravity measurements have an accuracy of approximately one microgal (Fairhead and Odegard 2002)

3.3 Instruments for gravity measurements

Gravity surveys are highly valuable for obtaining insights into subsurface geology, identifying geological structures, mapping underground resources, and supporting geotechnical and engineering applications. The primary instrument employed in gravity surveys is known as a gravimeter. While there are various types of gravimeters available, the ones most commonly used in gravity surveys include:

Relative Spring Gravimeters

Relative spring gravimeters (Figure 10) measure gravity by detecting the relative displacement of a mass-spring system resulting from variations in gravitational force. These instruments exhibit high sensitivity and are frequently employed in precise gravity surveys. The sensitivity of a relative gravimeter is typically in the range of 1 µGal/√Hz - microgals per square root of hertz (Tang et al., 2019).

Figure 10: Relative Spring Gravimeters (Carbone et al.2020)

Absolute Gravimeters

Absolute gravimeters (Figure 11) are more accurate but also more complex and expensive compared to relative spring gravimeters. These instruments directly measure the absolute value of the gravitational acceleration. The sensitivity of absolute gravimeters is significantly higher than relative gravimeters and is typically in the range of 0.001 µGal/√Hz (Tang et al., 2019).

Figure 11: Absolute Spring Gravimeters (Carbone et al., 2020)

Superconducting Gravimeters

Superconducting gravimeters (Figure 12) employ magnetic levitation as a means to gauge gravity. By leveraging the superconducting properties of specific materials, these gravimeters exhibit remarkable sensitivity, enabling the detection of even minute fluctuations in gravitational force. The sensitivity of Superconducting Gravimeters is typically in the range of nanogals per square root of hertz (nGal/√Hz) (Virtanen, 2006)

Figure 12: Superconducting Gravimeters (Carbone et al.2020c)

Microgravity Meters

Microgravity meters (Figure 13) are utilized to quantify exceedingly subtle fluctuations in gravity, commonly applied in engineering and environmental contexts. These meters demonstrate sensitivity towards gravity changes resulting from variances in subsurface density, including the existence of voids or subterranean structures. The sensitivity of Microgravity Meters is typically in the range of microGal (Saibi, 2018).

Figure 13: Scintrex CG-3 (left) and CG-5 (right) microgravity meters (Saibi, H. 2018)

3.4 Gravity Survey types

In gravity surveys, apart from the gravimeter itself, various instruments and tools are employed to ensure precise measurements and data acquisition. These may include:

1. Global Navigation Satellite Systems (GNSS) receivers and GPS equipment: These receivers provide accurate positioning information, facilitating the precise geolocation of survey points.
2. Surveying and leveling: For surveys covering smaller areas (1 km in length), it is essential to measure heights with a high level of accuracy, typically within ±1 cm. GPS technology cannot achieve this level of precision. Therefore, to obtain elevation the use of theodolite and levelling stave should be carried out.
3. Spirit levels: Spirit levels are utilized to ensure proper leveling and alignment of the gravimeter during measurements, enhancing measurement accuracy.
4. Data loggers: These devices record measurements obtained from the gravimeter, enabling data collection over extended periods and across multiple locations.
5. Field computers and software: These tools are employed for data processing, quality control, and real-time visualization of gravity data during field surveys, aiding in efficient data analysis and interpretation.

The use of these additional instruments enhances the accuracy, efficiency, and reliability of gravity surveys.

3.4.1 Land surface surveys

Land surface surveys for regional studies or reconnaissance purposes typically involve stations distributed in a grid pattern with kilometer-scale intervals. In regions with available data banks, these surveys may not be necessary as the data can be obtained from existing sources in discrete or gridded formats. On the other hand, detailed gravity studies for near-surface and upper crustal mapping require surveys with smaller station intervals, ranging from meters to hundreds of meters. In these cases, stations are distributed in a grid pattern or along profiles perpendicular to the anticipated longer dimension of the anomalies of interest. The profile spacing is generally limited to five times the distance between observations, considering terrain and access. The area covered and profile length are determined based on the maximum depth of the sources being investigated and the size and amplitude of regional anomalies. Station spacing should be carefully selected, considering factors such as anomaly characteristics, study objectives, noise levels, terrain, access, and available resources. The number of stations required for anomaly detection can be as low as three per anomaly, while the presence of significant noise may necessitate more complex spacing decisions. (Hinze et al., 2012)

3.4.2 Airborne surveys

Airborne surveys are specifically designed based on the anticipated gravity anomalies and survey objectives. The selection of an appropriate aircraft is crucial, considering the objectives, terrain, and access to the study region. Typically, single, or twin-engine aircraft capable of slower speeds (around 50 to 100 m/s) are chosen to achieve the desired accuracy-to-resolution ratio. Safety considerations may lead to the use of helicopters in regions with steep topography or continuous cloud cover. Onboard magnetic sensors and recording equipment supplement gravity measurements but are determined by the gravity requirements.

Gravity observations are made along parallel lines perpendicular to the expected strike of the anomalies, with orthogonal tie lines spaced 5 to 10 times the line spacing for quality control and data processing. Flight line spacing depends on the required accuracy and resolution, with higher accuracy and shorter resolutions necessitating closer line spacings. Altitude above the ground is chosen to maximize resolution and anomaly visibility while adhering to safety regulations and turbulence constraints. Flight altitudes are typically a few hundred meters, and in regions with topographic variations, the survey can be draped over the terrain to enhance resolution. Navigational considerations depend on the allowable errors in altitude and position, which dictate the survey's navigational requirements. (Hinze et al., 2012)
Real-time quality control is vital for data acquisition and processing in airborne gravity surveys to achieve survey goals.

3.4.3 Satellite gravity mapping

Satellite-altitude gravity observations provide valuable boundary conditions for interpreting near-surface gravity variations. While a model based on a single altitude slice only captures behavior within a station interval due to measurement errors, a model combining satellite-altitude and near-surface observations offers a more comprehensive understanding of gravity field variations across unsurveyed altitudes. This joint model enhances interpretation of anomalous subsurface mass variations. Geodesists conduct satellite-altitude gravity surveys to map geoidal undulations and temporal variations in low-order gravity components. The GRACE and GOCE missions (Anderson and Cazenave, 1986; Jäggi et al., 2011; Visser, 1999) collect state-of-the-art satellite gravity data at altitudes of approximately 450-500 km and 270 km, respectively. The satellites operate in near-Sun-synchronous orbits, completing each orbit in about 96 minutes. The ground tracks become tangential to pole-centered holes or coverage gaps as they approach the polar regions due to the orbit inclination relative to the Earth's equatorial plane (Hinze et al., 2012).

3.5 Data collection for gravity surveys

Successful acquisition of gravity data for exploration relies on careful selection of instruments, survey design, measurement procedures, and reduction and interpretation methodologies aligned with the study objectives. To ensure the intended goals are met, comprehensive quality control procedures are necessary at every stage of the process. Additionally, a strong understanding of gravity principles and their application to exploration is essential (Hinze et al., 2012).

To collect gravity data, one person can perform the task, but two people are typically needed to determine the location of gravity stations, including latitude, longitude, and elevation. The first step is to select a suitable gravity meter, considering the varying accuracies offered by different manufacturers.

After selecting the gravity meter, a grid or profile is laid out over the area of interest. In order to do this, the distance between gravity stations must be measured, and each station's position and elevation must be surveyed. Station spacing ranges from 0.5 to 5 meters for engineering and environmental studies but can be larger (up to 100 meters) for studies focused on bedrock topography (Mickus, 2003).

To account for instrument drift and remove the effects of earth tides, a local base station is established, where gravity readings are repeated at regular intervals (usually every 0.5 to 1 hour). This helps ensure accurate measurements over time.

In detailed surveys, the earth tide effect must be considered as it can have a significant impact on gravity values. Drift curves are used to obtain base readings corresponding to the time each station was measured. The readings are initially obtained in gravity meter units and then converted to milligals using manufacturer-supplied calibration constants.

During fieldwork, in absolute gravity surveys, the gravity meter is carefully leveled using leveling bulbs to align it with the local vertical direction. To ensure accuracy, temperature variations are monitored, and a waiting period of one to two hours is observed for meter stabilization. Multiple readings are taken at each station, checking for differences below a threshold of 0.01 mGal, to minimize random errors and ensure reliable and precise measurements. In relative gravity surveys, the focus is on measuring gravity differences between

different locations, not absolute gravity values. The procedures involve establishing a baseline, using gravity meters for measurements, calibrating the instruments, ensuring meter stability, and accounting for environmental factors.

In addition to gravity readings, the horizontal position (latitude, longitude, or x and y distances) and elevation of each gravity station must be determined. This can be achieved through electronic distance meter (theodolite) surveys or total field differentially corrected global positioning surveys (GPS). For general geological surveys, a precision of 0.01 mGals is typically sufficient. In this case, elevations should be measured within 3 cm (where a 3 cm change in elevation corresponds to 0.01 mGal). High accuracy is crucial for critical tasks in engineering geology and archaeology, where for microGal precision, elevation measurements must achieve an accuracy of 3mm (a 3mm change in elevation corresponds to 1 µGal).

Lastly, topographic changes and the effects of nearby buildings on gravity stations are considered. Techniques such as recording elevation changes in quadrants or using laser positioning guns are employed to determine elevation changes. LiDAR technology enhances the understanding of topographic changes, effects of nearby buildings, and accurate recording of elevation changes. Additionally, the gravitational effects of buildings are accounted for in microgravity surveys by modeling them as rectangular prisms (Loj and Porzucek, 2019).

Overall, gravity data collection involves selecting appropriate equipment, establishing survey stations, conducting measurements, and considering factors like instrument drift, earth tides, and topographic effects.

3.6 Factors Affecting Gravity Measurements

The measurement of gravitational acceleration at any point is influenced by several factors that are associated with either the location or the instrumentation used. These factors must be taken into account and corrected when analyzing gravity data. The following are the effects of these factors:

Latitude: Gravity varies with latitude, with the maximum difference occurring between the equator and the poles. The gradient of this change, known as the latitude effect, is highest at 45° latitude, where it is approximately 0.8 mGal/km. At the poles, the difference in gravity is greater, amounting to around 5000 mGal.

Elevation: Changes in elevation have a significant impact on gravity measurements. Modern instruments are

sensitive enough to detect even small changes in elevation. The difference in gravity between sea level and the peak of Mt. Everest is roughly 2000 mGal.

Slab Effect: When ascending in elevation, there are usually intervening rocks and soils between the measurement point and the starting location. The gravitational attraction of these materials counteracts the effect of elevation change. To correct for this, a factor known as the Bouguer correction is subtracted. The Bouguer correction is calculated by multiplying the elevation (in meters) by the density of the intervening materials (in g/cm^3) and is typically around 0.3 mGal/m.

Topography: Nearby topographic features such as hills or valleys can introduce significant gravity effects, although they are generally limited to approximately 1.0 mGal. Correcting for these effects can be complex but is crucial when conducting surveys in regions with steep topography.

Earth Tides: Tidal forces exerted by the moon and the sun can influence gravity measurements, contributing variations of up to 0.3 mGal. These effects are typically accounted for by taking multiple measurements at a base station throughout the survey. Since the 1990s, tidal effects have been computed using the Longman formula (1959). This formula incorporates various constants, such as distances, masses, ellipsoidal parameters, and orbital values, along with conveniently rounded values for time calculations (Amarante and Trabanco, 2016). In most of today's modern gravimeters the correction of earth tide effects is automatically included in measurement software.

Lateral Density Variations: Large-scale structural anomalies, such as basin and range geology, can produce gravity anomalies ranging from 100 to 500 mGal. In the context of oil exploration, notable targets like salt domes may cause anomalies of approximately 10 mGal, while ore bodies in mineral exploration can create anomalies around 1 mGal. In geotechnical applications, anomalies of around 20 μGal may be encountered.

Effects of a Moving Platform: If the measurement instrument is in motion during data acquisition, the acceleration caused by the instrument's movement on a rotating sphere must be considered. These additional accelerations can be particularly significant in airborne surveys or when measuring from a moving ship, even in mild sea conditions.

In relative gravimeters, changes in the elastic properties of the measuring spring, also known as drift, occur. Drift refers to both long-term permanent changes in the spring caused by factors like temperature and pressure variations, as well as short-term temporary changes. These fluctuations can affect the accuracy of the measurements over time.

3.7 Gravity Data Processing

The gravity readings acquired during a gravity survey capture the combined gravitational field generated by all masses within the Earth and the influence of the Earth's rotation. Interpreting gravity data requires the removal of gravitational effects unrelated to changes in subsurface density. These effects encompass variations in latitude, elevation, topography, building structures, and earth tides. By eliminating these known gravitational influences, a clearer understanding of the subsurface density changes can be obtained (LaFehr, 1991).

Latitude correction

Latitude correction is a necessary adjustment made to account for the variation in the acceleration due to gravity caused by the Earth's shape and rotation. Gravity decreases from about 983,000 mGal at the pole to about 978,000 mGal at the equator. About 3400 mGal of this decrease results from a difference in centrifugal acceleration; the rest is due to polar flattening. The International Gravity Formula (GRS67, Geodetic Reference System, 1967) for computing the expected value of gravity on the reference ellipsoid (a near-sea-level mathematical surface that closely approximates the Earth's shape) is:

$$g(\Phi) = 978031.846 \cdot (1 + 0.005278895 sin^2\Phi + 0.000023462 sin^4\Phi) \quad (3)$$

Where Φ = Latitude

Free-air correction

The free-air correction is utilized to compensate for gravitational discrepancies resulting from variations in elevation between observation locations. By incorporating a correction value of 0.3086 *h* mGal (where h represents the elevation in meters), the influence of the $1/r^2$ dependency is considered. When measurements are conducted at higher elevations, they tend to yield smaller values. Therefore, to account for this effect, it is necessary to add the correction for higher elevations.

Bouguer correction

By applying this adjustment, the free-air value is rectified to consider the presence of material between the reference elevation and the measurement location. When the measurement point is positioned at a higher elevation above the reference, the quantity of material encountered increases (resulting in a greater effect). Consequently, it is necessary to subtract a specific value *0.04191·h·d* mGal (*h* in meters, *d* in *g/cc*) from the

reading. This derivation process involves assessing the impact of a single point, followed by integration along a line, further extending to a sheet, and finally encompassing a slab.

Topography, or terrain correction

This correction factor accommodates the additional mass present above (such as hills) or the reduced mass (such as valleys) beneath the elevation of a specific reading. Traditionally, this manual adjustment involved utilizing a "Hammer chart" and reference tables (Hammer, 1939; Jentzsch et al., 2000), albeit with limited accuracy. However, contemporary approaches rely on software equipped with digital terrain models (DTM) obtained from governmental or third-party sources. These advanced methods enhance precision and efficiency in accounting for the effects of varying mass distribution on gravity measurements.

Earth-tides

Tidal variations occur at a gradual pace, which allows them to be addressed as part of the drift correction process during most surveys. This involves capturing measurements at a base station every few hours, effectively accounting for the influence of tidal fluctuations.

Eötvös correction

This correction is required when the instrument is situated on a mobile platform, such as a ship or aircraft. It accommodates the centrifugal acceleration arising from the motion on a rotating Earth.

The relationship is defined by the equation (Jentzsch et al., 2000):

$$a_r = 2\omega u \cos\varphi + \frac{u^2 + \vartheta^2}{R} \tag{4}$$

where:

a_r = relative acceleration

ω = rotation rate of the earth

u = velocity in longitudinal direction (east-west)

ϑ = velocity in latitudinal direction (north-south)

φ = latitude where the measurements are taken

R = radius of the earth

At mid-latitudes, this correction amounts to approximately 7.5 mGal for every 1 knot of east-west motion.

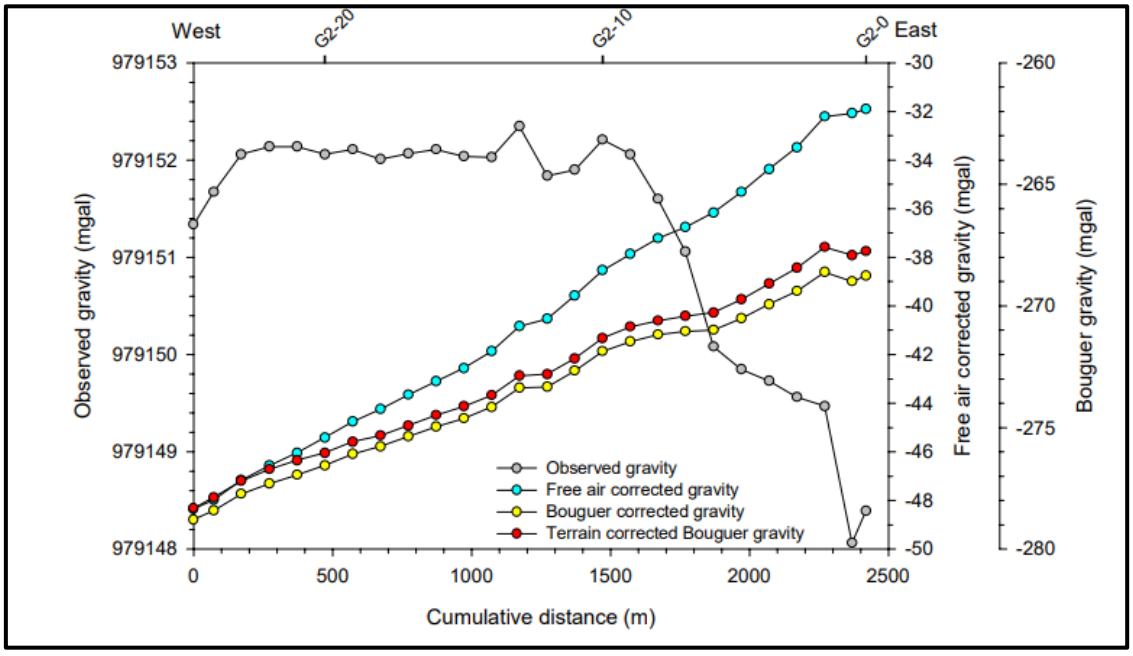

Figure 14: The diagram illustrates the impact of individual corrections on a surveyed short line. It presents the raw data with drift correction, as well as the effects of each correction factor. Typically, the Bouguer anomaly graph (highlighted in yellow) would be utilized for final interpretations. This data was collected during the Astronaut Geophysical Training in Taos, New Mexico, in the summer of 1999 (Bauer et al, 1999)

Compiled Maps

The collected gravity measurements are typically processed to obtain a complete-Bouguer or isostatic gravity anomaly. These processed data provide a clearer representation of the gravity variations by accounting for factors such as topographic effects and the Earth's crustal density variations.

To generate a gravity map, the processed measurements are transformed into a grid format. This gridding process converts the randomly spaced data into a representation of the gravity field at equally spaced locations on a regular grid. The grid interval chosen depends on the average distance between gravity stations. Striking the right balance is crucial: a grid interval that is too large would disregard valuable information from the original dataset, while a grid interval that is too small could lead to fragmented anomalies, resulting in a poor representation of the true gravity field.

Gravity anomaly maps are commonly presented using color figures or contour line maps. In color figures, warm colors represent higher gravity values, while cool colors represent lower values. Contour line maps connect points with the same gravity value, allowing the identification of regions with consistent gravity anomalies. Both methods are valuable for understanding variations in gravity across different areas (Hill et al., 1997).

4. Practical part - Creation of gravity anomaly maps of Ethiopia and Linsser Indications

Since the early 1960s, the gravity field of Ethiopia has been the subject of investigation with the goal of understanding the overall crustal structure of the region. Previous studies have primarily focused on examining the crustal structure of two specific areas: the Main Ethiopian Rift (MER) and the northeastern Afar region. These studies have revealed that the MER region exhibit a regional Bouguer gravity high, indicating crustal thinning as the mantle has higher densities (Mickus et al., 2007; Mohr and Rogers, 1966)(Figure 20)

The thickness and density distribution of the crust of MER were measured by Mahatsente et al. (1999, 2000) and Jentzsch et al. (2000). They distinguished a 31-kilometer-long zone of crustal thinning in the main rift, which is consistent with hypothesized intrusions in the upper crust. The crust thickens to around 50 km on the northwest and southeast faces of the major rift. Mahatsente et al. (2000) came to the conclusion that continental crust forms the upper portion of the main Ethiopian rift based on the magnitude and features of these intrusions. The intrusion associated with a gravity maximum over the MER becomes thinner towards the north and has a width of around 20 km in the northern MER.

4.1 Datasets and Gravity Data Processing

The gravity data utilized in this research includes two datasets:

1) The airborne gravity data (ABGD) dataset acquired by the Danish National Space Center during the period 2006 to 2008 along flight lines 10 nautical miles apart, around 18 km, at an elevation of 2000 m allowing for large and medium scale geological research with a resolution suitable for resolving geological structures with size of several kilometres (Figure 15). The heights and gravity readings obtained from the airbourne gravity surveys have an estimated accuracy of 3-7 cm and 2.7 mGal, respectively.

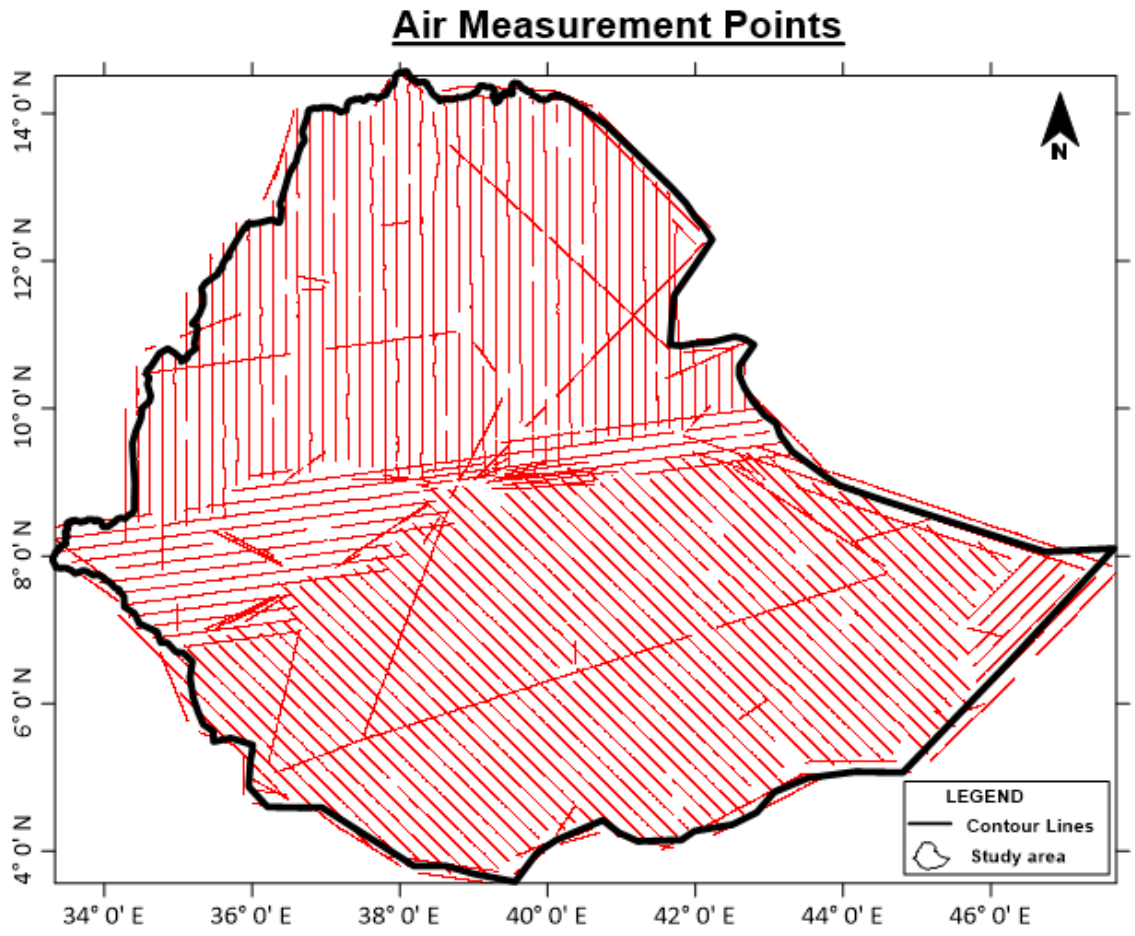

Figure 15: Gravity measurement points in airborne gravity dataset (ABGD)

2) The second dataset is obtained from land surface surveys - a comprehensive dataset consisting of more than 48,002 gravity measurements from both land and sea has been compiled (Figure 16). These data points have been generated by various companies, research institutions, and are archived in international organizations and geological survey databases. In the early 1970s, initial studies were conducted on the Afar region of Ethiopia, Djibouti, the western escarpment, and the highlands of Ethiopia (Makris et al., 1972). The Geophysical Observatory of Addis Ababa University also conducted preliminary works during that time Additional gravity data collection efforts were carried out by (Ebinger and Ibrahim, 1994) and (Ebinger and Hayward, 1996) in the southern rift and Afar area. The Geological Survey of Ethiopia (GSE) has played a significant role in contributing to gravity research through various research projects, such as the SAREC/ESTC (1988-1994) and ETHIO-NOR programs. The GSE continues to conduct gravity campaigns as part of its ongoing efforts.

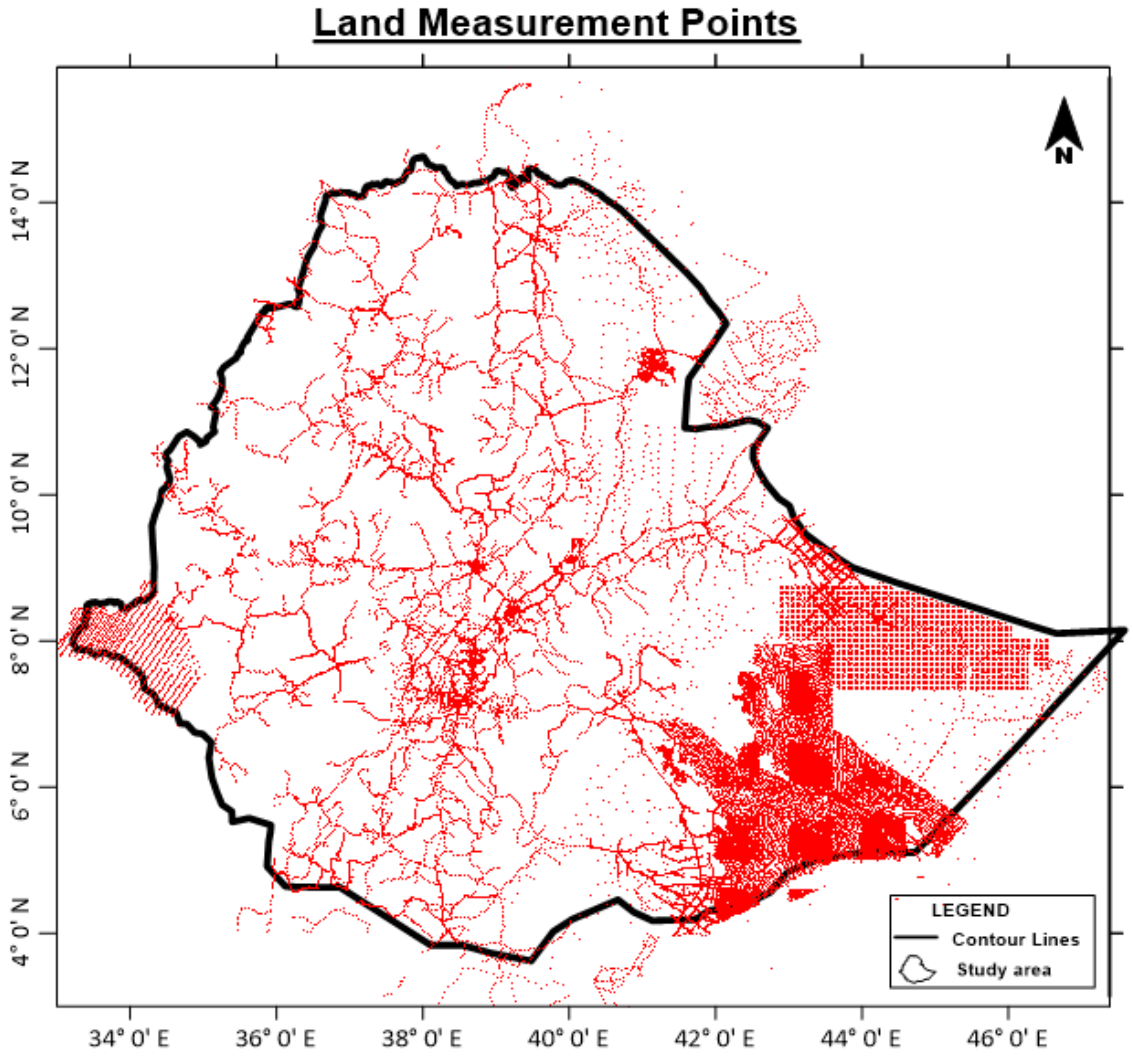

Figure 16: Localization of 48002 gravity stations from SAREC/ESTC and ETHIO-NOR programs

The land and airborne bouguer anomaly maps reveal a broad regional negative Bouguer anomaly over the Ethiopian region. The anomaly reaches a maximum of 20 mGal in the northeastern region of Ethiopia and a minimum of -280 mGal in the MER as its amplitude grows with a reduction in topographic relief. The Bouguer anomaly maps have a difference of approximately -15 mGal between measurements taken on land and those collected via airborne methods (Figure 17). While both anomaly maps demonstrate similarities in the distribution of low and high geological structures, a slight difference emerges in the southern part of Ethiopia. This dissimilarity could be attributed to the scarcity of gravity measurement stations within the land survey dataset and the Bouguer anomaly map is depended on interpolation due to the limited availability of measurement points. In large scale investigation both the data set can be used as the disparities between them are not likely to exert a significant impact.

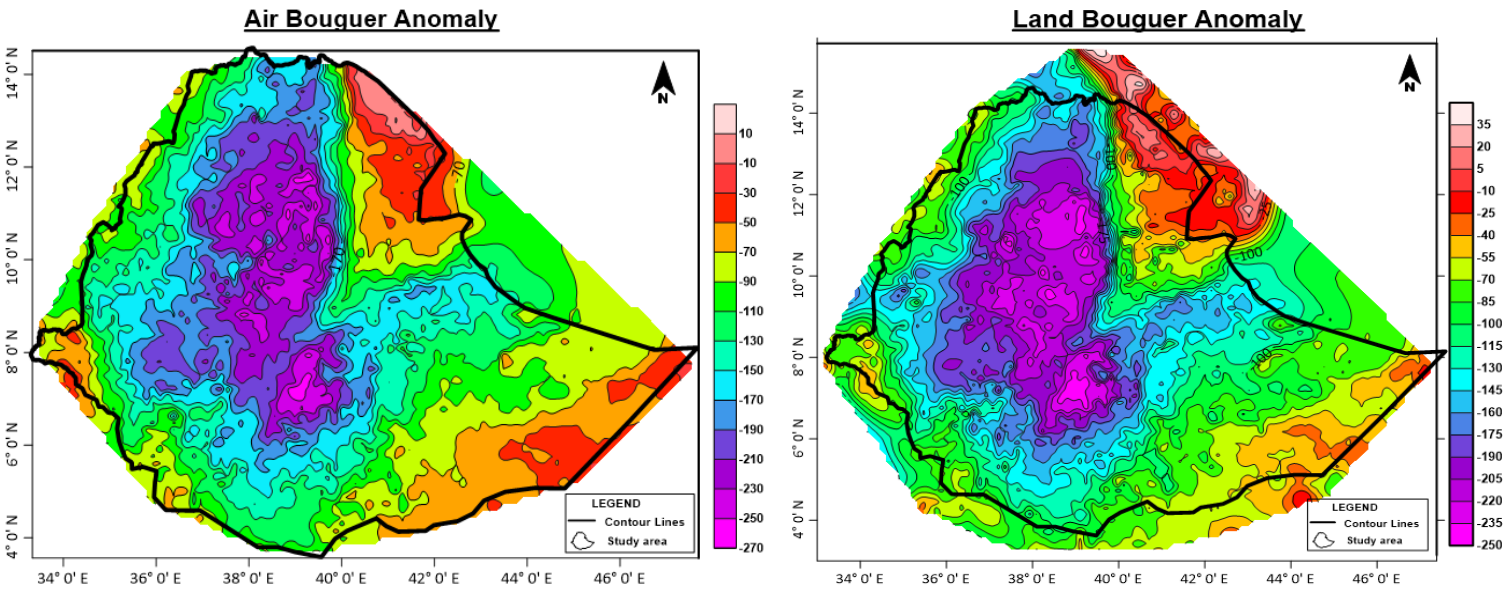

Figure 17: Airborne Bouguer Anomaly Map (left), Land Bouguer Anomaly Map (right)

Several corrections were applied to the observed gravity data. Firstly, a correction for drift was implemented to account for instrumental variations over time. Secondly, latitude correction was performed to consider the influence of the Earth's rotation and the location of the measurements. Additionally, free air correction was applied to eliminate the effects of height variations relative to the chosen reference surface, using the 1967 international gravity formula.

Furthermore, a Bouguer correction was implemented to compensate for the gravitational effect of mass between the surface and reference level. This correction factor accounts for the density variation of subsurface geological structures. A reduction density of 2.67 g/cm^3 was used, and the datum was set at sea level.

Terrain corrections according to the Hammer's scheme (Hammer, 1939) were computed using the Shuttle Radar Topography Mission (SRTM) Digital Elevation Model (DEM) provided by the U.S. Geological Survey (EROS, 2018). Analysis of the statistics reveals that approximately 67% of the data coverage had terrain corrections ranging from 0 to 0.419 mGal. About 23.7% of the data fell within the range of 0.419 to 1.88 mGal. Another 5.3% of the data had corrections ranging from 1.88 to 3.356 mGal, while 2% of the data fell within the range of 3.356 to 4.82 mGal. Lastly, less than 1% of the data required corrections greater than 6.29 mGal. These terrain corrections were applied to account for the influence of the topography on the gravity measurements and ensure accurate interpretation and analysis.

To visualize the results, the computed complete and Bouguer anomaly values were gridded and used to generate a comprehensive map displaying the complete Bouguer anomaly (Figure 17).

Another dataset utilized in this research originates from the mapping activities conducted by the Danish National Space Center during the period of 2006 to 2008 (Olesen and Forsberg, 2007; Belay et al., 2022). The data were collected through airborne campaigns. These campaigns involved recording measurements along flight lines that were approximately 10 nautical miles apart (approximately 18 km) and at an approximate flight clearance of 2000 m. The average measurement error (of the whole dataset), determined through flight line crossings, was found to be 2.7 mGal. To convert the measured data from the flight elevation to the Earth's surface, a downward continuation of the gravity field was performed, accounting for the approximate topographic surface at 2000 m. This calculation was carried out using algorithms available in the Oasis Montaj software. Corrections for topography were computed using the ETOPO1 digital elevation model.

Finally, the resulting Complete Bouguer Anomalies (CBA) were further recalculated to a regular grid using the kriging algorithm, which was implemented in the Golden Software Surfer mapping software (Figure 17).

4.2 Bouguer Anomaly

Figure 18 and 19 showcases a Bouguer Land gravity anomaly map of the Ethiopian region, utilizing data from 48,002 gravity stations, any of the two datasets can be used for a large-scale study because in such scale they are show no significant difference. The Bouguer gravity anomalies in Ethiopia span a range from -260 to 20 mGal. Upon a cursory examination of the Bouguer gravity anomaly map (Fig. 19), the gravity field can be categorized into four primary anomaly regions. 1-The Main Ethiopian Rift (MER): This region exhibits a regional gravity maximum that gradually widens and intensifies towards the north. 2-The Southern Ethiopian Rift (SER): Gravity anomalies in this area increase towards the south. 3-The eastern Ethiopian plateau: These regions display lower Bouguer gravity anomalies. 4-The western Ethiopian plateau: These areas feature the lowest Bouguer gravity anomalies. Additionally, the Afar depression stands out as a distinct region where the Bouguer gravity anomalies increase from the MER towards the north.

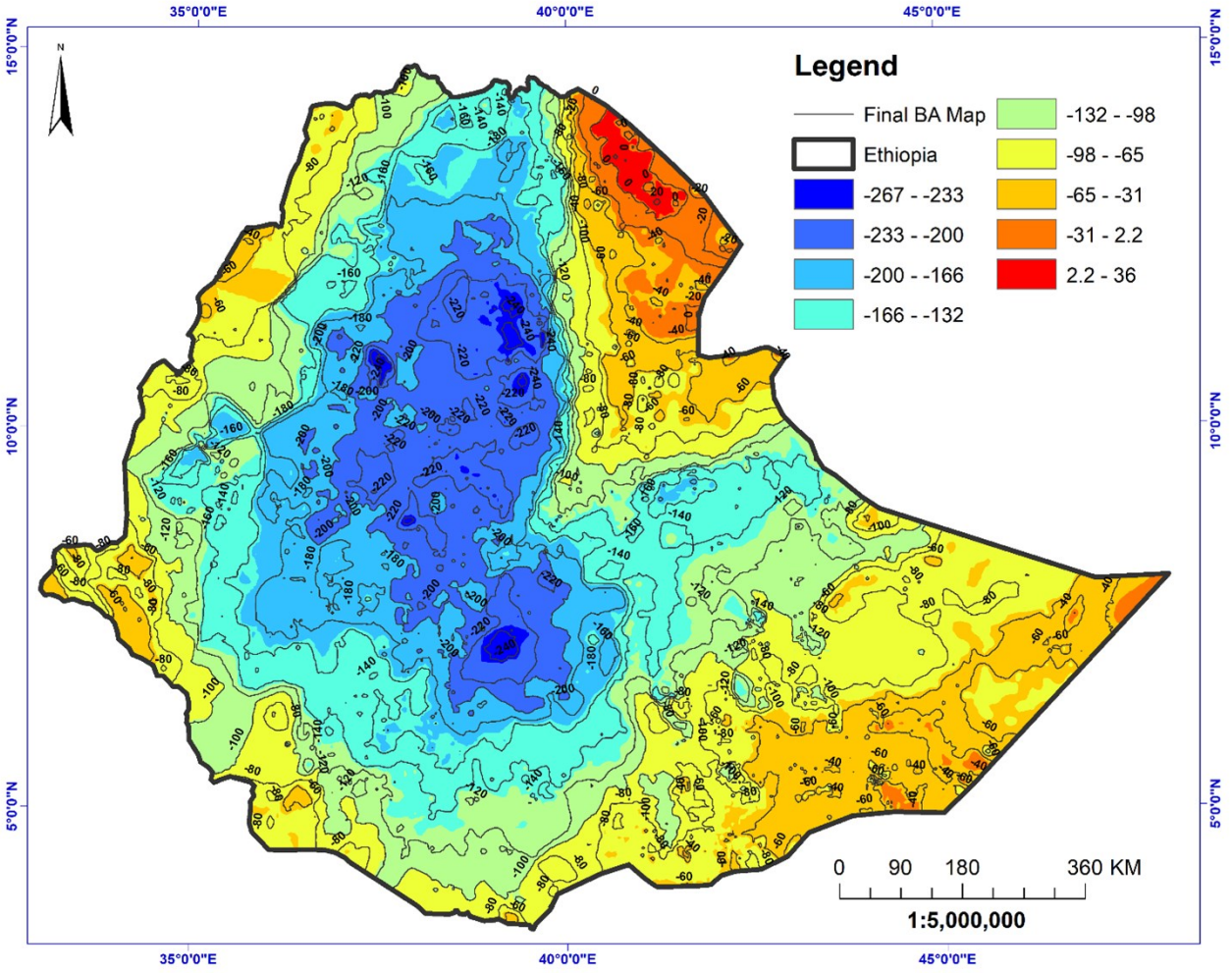

Figure 18: Land Bouguer anomaly contour map of Ethiopia

The gravity maximum observed over the Main Ethiopian Rift (MER) is attributed to either a thinned crust, igneous intrusions, or a combination of both. The anomaly values decrease from north to south, ranging from -80 to -220 mGal (Figure 18). This decrease is a result of the increasing depth to the MOHO boundary and an elevation in the density of the crust/upper mantle towards the southern region (Nigussie et al., 2023). In MER, the average anomaly value ranges from approximately -200 to -240 mGal, with a significant positive gradient starting at the Boset magmatic segment (Figure 18). The Boset magmatic segment exhibits a notable amplitude gradient in the Bouguer gravity field, likely due to variations in crustal thickness and density between the southern Afar region and the MER (Mickus et al., 2007).

Bouguer gravity anomaly map reveals that a significant portion of the western plateau in Ethiopia is characterized by a gravity low with a long wavelength. It covers a considerable area extending from Chencha (around 37° E and 6° N) in the southern part of the western plateau, along the Gurage highlands (around 38° E and 8° N) within the western margin of the Main Ethiopian Rift (MER), and the Blue Nile area further north of Lake Tana. The gravity low in the western plateau follows a northeast-southwest trending elliptical pattern that corresponds to the elevation of the plateau (Figure 19) and thus thicker layer of low density material and higher depth of MOHO − up to approximately 50 km (Kassa et al., 2021).

On the other hand, the eastern plateau is associated with another distinct gravity low anomaly. Much of the elevated regions, exceeding 3000 meters above sea level, exhibit a broad negative anomaly in gravity.

The Afar triple junction displays significant northeast-southwest positive anomalies, aligned with the Ethiopian rift section. Erte Ale (EA) region exhibits a north-northwest to south-southeast positive anomaly, separated from the southern Afar anomaly Figure 19. The southern Afar reduced gravity anomaly might be a sign that the Red Sea rift is coming to a close. A comparatively negative anomaly between Erte Ale and the Red Sea is shown in the Danakil horst. An further positive anomaly has been identified in the Turkana rift, coinciding with Lake Turkana and displaying a north-south orientation.

In Figure 19 the southern Ethiopian rift (SER) is depicted with gravity anomalies. The Anza graben is clearly distinguished by a northwest-southeast trending negative gravity anomaly, displaying a significant decrease of -60 mGal, accompanied by relatively larger negative anomalies of around -100 mGal. The Turkana rift, located near Lake Turkana, exhibits a notable extent of low negative gravity anomalies (-80 mGal). Moving southeast into the Turkana graben, a lower negative gravity anomaly of approximately -60 mGal is observed (Figure 19).

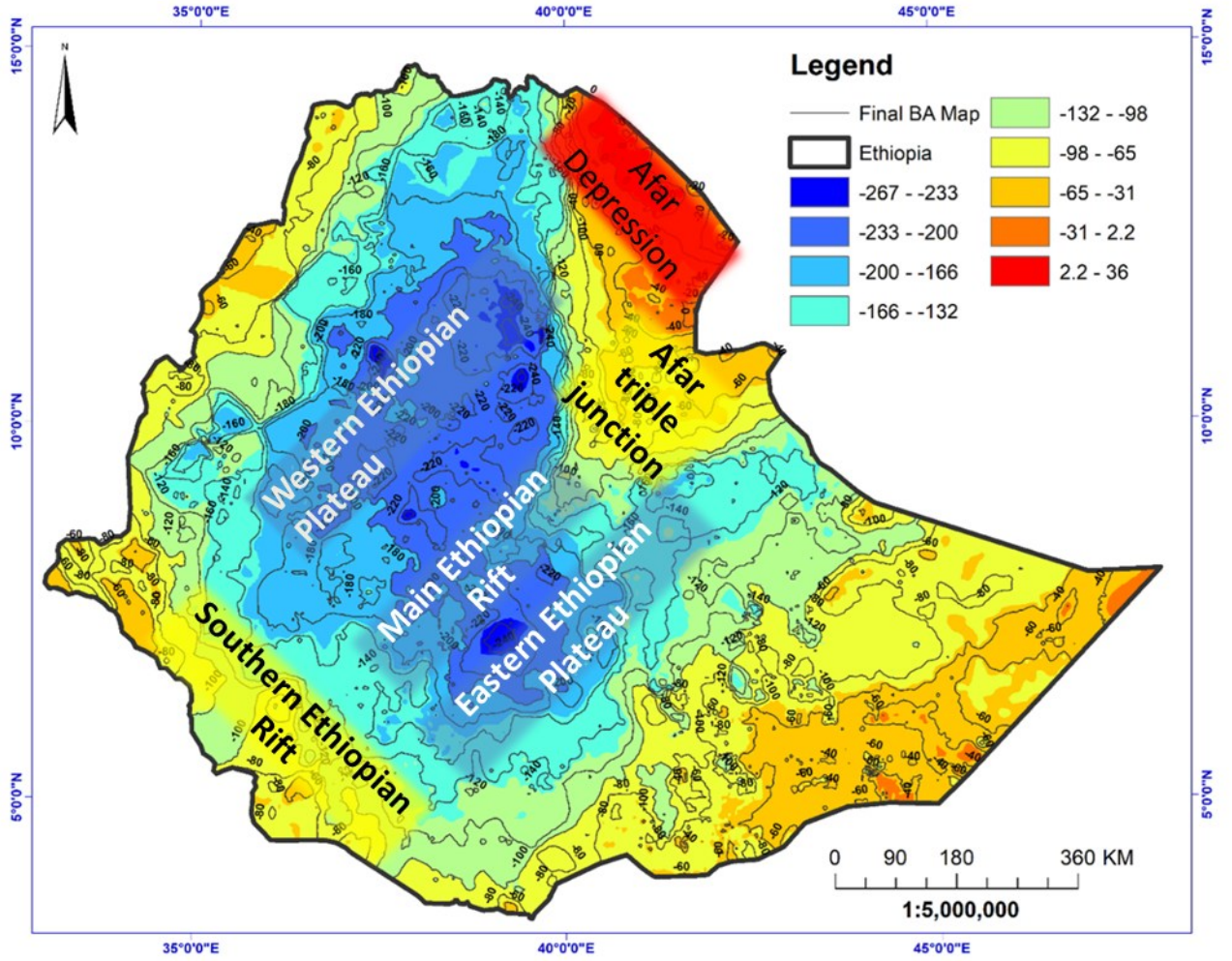

Figure 19: Land Bouguer anomaly contour map of Ethiopia with identifications

4.3 Detailed study of the Sidama and Gedeo zones

4.3.1 Linsser indications of vertical density contacts

The application of gravimetric surveys allows for the investigation of the geological characteristics of a region, including the detection of brittle tectonic deformations and faults (Bielik et al., 2002; Linsser, 1967a). Gravity gradients frequently delineate the boundaries between geological units characterized by variations in density. These gradients serve as prominent indicators of tectonic features on a gravimetric map. Their strength correlates with the disparities in density, the amplitude of the step change, and the fault's inclination. In practical applications, the density boundary (fault) is approximated using a simple two-dimensional geometric body with infinite dimensions along the fault (Bielik et al., 2002; Griffiths and King, 2013)

Therefore, one method of density contacts detection relays on computing the gradient of the gravity field. The essence of this method is the fact that the change (gradient) of the gravity field is the highest on the boundary between two blocks with different densities. The gradient function is obtained by deriving the measured gravity data (Vz) either concerning the x and y axes (horizontal gradient - Vzx or Vzy - HG) or the z-axis (vertical gradient - Vzz - VG). These derivatives can be determined using finite differences. The resulting maps depict the positions of inflection points (identifying maxima of the gravity field gradient amplitude) or isolines of the gradient magnitudes (Nettleton, 1971; Pick et al., 1973).

Another method often used in potential methods interpretation are calculations of transformed maps which differ from the original maps of total Bouguer gravity anomalies by emphasizing certain components that are of interest (Bielik et al., 2002; Šefara, 1973). Transformations do not provide new information but can extract and amplify existing details in the original map. The choice of transformation method depends on whether the faults being studied are shallow or deep. For shallow faults, the interpreter applies a transformation that emphasizes anomalies with short wavelengths and vice versa. The residual anomaly at each point is calculated as the mean value within a circular area (Griffin 1949; Pick et al. 1973). By analyzing the anomalies in the transformed map, it is possible to indirectly determine whether the fault structure is shallow or deep and estimate its depth.

However, as pointed out by Linsser (1967) on complex structures involving high number of density-different

blocks these ways for identification of density contacts can lead to suboptimal or even misleading interpretations. Therefore, he came with another technique which is better suited to map these structures in a better way − direct indications of density contrasts (Linsser, 1967), lately called Linsser indications of density contrasts.

4.3.2 Methodology

The Linsser's method involves filtering the anomalous field by comparing a pre-determined theoretical anomalous effect with the measured gravity field. The model used is a vertical density boundary, which is suitable for approximating linear geological structures. The output data defines indications of vertical density boundaries (Bielik et al., 2002). If these indications align along specific lines, they are interpreted as vertical or slanted density boundaries characteristic of linear faults. Non-linear indications on the maps suggest the presence of three-dimensional bodies rather than linear structures.

Determination of the Throw of the Fault

To determine the throw of a step fault, four parameters are considered: depth of burial for the high and low blocks, the fault's hade (inclination), and the density difference between upper and lower rock material. Small gravity undulations require careful examination (Linsser, 1967a).

To simplify the analysis, a master curve is defined using a simplified geological model. At an arbitrary depth, a step fault with a certain throw (±1 km) and an effective density difference (± 1 g cm^{-3}) is chosen. The total gravity effect of approximately 42 mGal is standardized by the value E = 1. The "effect" (E) represents the product of the fault throw and density difference, measured in km g cm^{-5}. This methodology helps quantify the throw of the step fault based on its gravitational effects and provides insights into the subsurface geological structure (Linsser, 1967b).

Determination of the Fault Location

To determine the location of a fault, the value E is calculated by comparing the measured gravity profile with various master curves (templates). The interpreter shifts the template horizontally until the best fit is achieved, revealing the fault's location. This process is simulated using a computer to convert the optical analysis into a mathematical one.

The coincidence value (C) measures how closely the measured gravity profile matches the theoretical profile of the fault. C is equal to 100% when there is an exact match. The value of C shows a pronounced maximum directly above the step fault and decreases laterally along steep planes. This methodology helps pinpoint the location of the fault based on its gravitational effects and provides valuable information about subsurface geological structures (Linsser, 1967b)

Determination of the Fault Direction

The fault direction is determined by the interpreter drawing profiles perpendicular to the fault. This process involves marking a point and creating a vertical axis around which a vertical plane is rotated. The rotating plane intersects the gravity values surface at different angles, with the plane perpendicular to the fault showing the strongest effect, while the plane in the fault direction shows no influence.

The value E is calculated as a function of the rotation angle. The angle corresponding to the extreme value of E defines the direction perpendicular to the fault, and the value C is determined for this direction, indicating the coincidence between the measured gravity profile and the theoretical fault profile.

If multiple faults cross the axis, several relative maxima are obtained. By determining all relative maxima, all fault directions that intersect the observed point are identified. This methodology helps accurately determine the direction of the fault and provides valuable information about the subsurface structural orientation (Linsser, 1967b).

This method was then further modified and improved by Šefara (Šefara, 1973; Šefara and Obr, 1973). One of their major improvements is that they search for continuous density indications spreading over larger area (three adjacent grid lines in their version) which leads to less scattered indications and more focused images.

4.3.3 Gravity Data

The gravity data used for (relatively) small-scale investigation of the Sidama and Gedeo zones were taken solely from the airborne gravity dataset (Figure 21) rather than from the land one (Figure 22) as the land dataset has large areas not covered by gravity stations and the distribution of gravity measurements is extremely irregular (Figure 23 and 20).

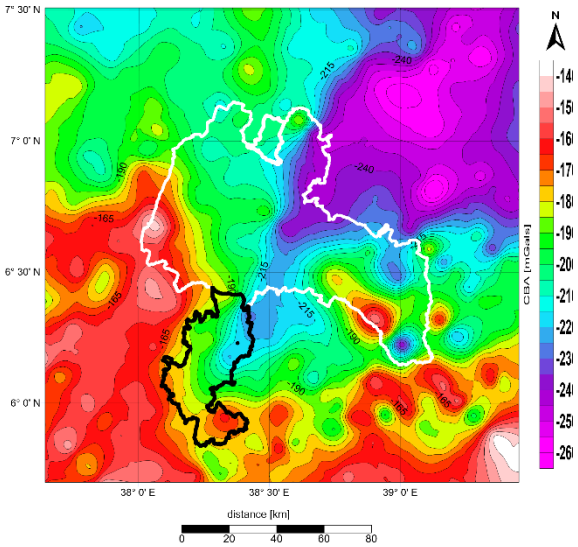

Figure 20: Airborne Bouguer Map of Sidama (white boundary) and Gedeo (black boundary)

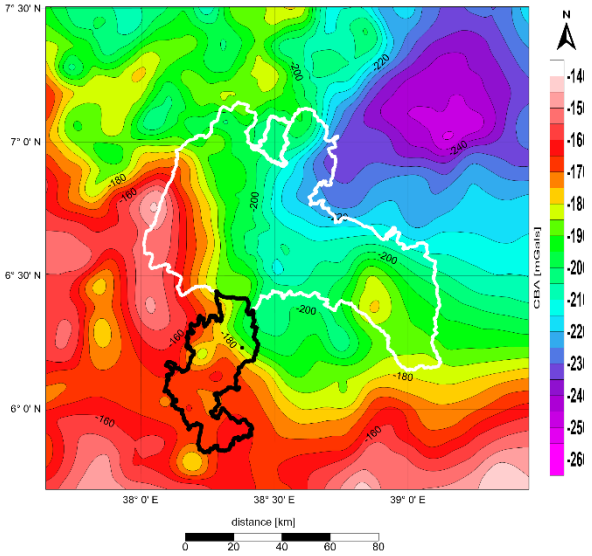

Figure 21: Land Bouguer Map of Sidama (white boundary) and Gedeo (black boundary)

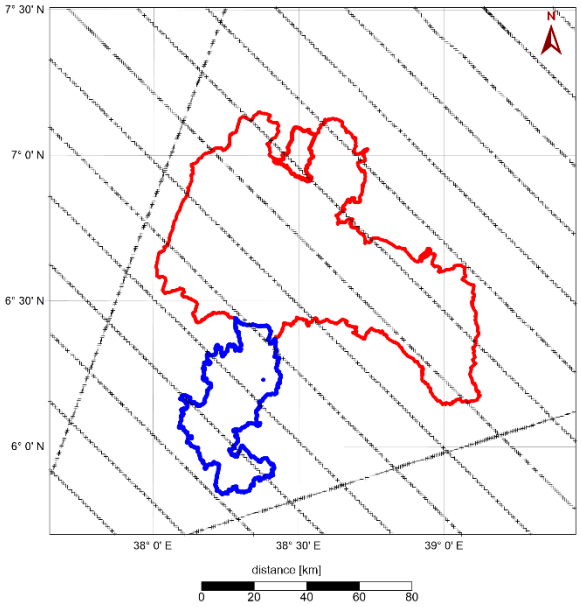

Figure 23: Land gravity stations maps Sidama (red boundary) and Gedeo (blue boundary) zones

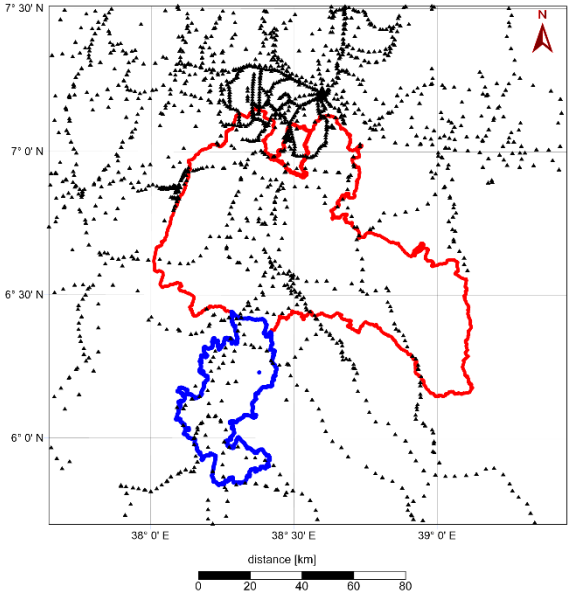

Figure 22: Airborne gravity flight maps Sidama (red boundary) and Gedeo (blue boundary) zones

The entire region displays a notable transition between a profound gravity low, plunging below –250 mGal, situated to the northeast of the Sidama boundary, and a pronounced gravity high, surpassing –140 mGal, observed on the western and southern sides of both zones. This elevated gravity is intricately linked to the ongoing tectonic rifting processes within the Main Ethiopian Rift, encompassing asthenospheric upwelling and mantle intrusion (Mahatsente et al., 2000). These long wavelength gravity anomalies predominantly signify variations in the Moho's depth, spanning from 42 km in the northern and northeastern sectors to 36 km in the southern and southeastern regions (Kassa et al. in 2021). The presence of gravity lows is attributed to the greater thickness of upper crustal rocks with relatively low density. The Bouguer anomaly indicates the extension of this group towards the south into the Gedeo Zone.

The high gravity values observed in the southeastern portion of the Sidama Zone, reaching up to –150 mGal, are likely attributed to the presence of high density Precambrian crystalline units close to the surface. In contrast, the Neogene basaltic lavas and pyroclastics exhibit comparatively lower densities due to the high porosity of the effusive rocks and consequently lower gravity values. In the western part of the Sidama Zone, a substantial layer exceeding 1 kilometer in thickness, composed of young, late-rift trachyte and rhyolite lavas with lower densities, contributes to a decrease in measured gravity acceleration. These lava formations, in conjunction with rift sediments, likely account for the slightly negative residual anomaly observed at the rift center (Mahatsente et al. 1999).

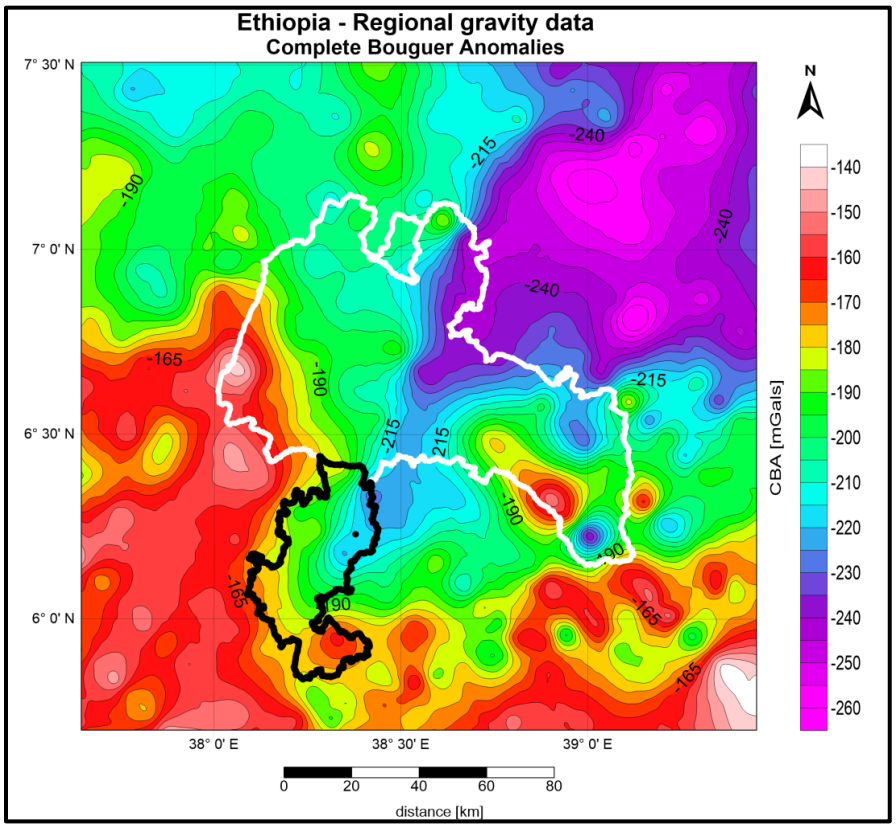

Figure 24: Airborne Bouguer gravity anomaly map of the Sidama (white boundary) and Gedeo (black boundary) zones

4.3.4 Linsser Anomaly of Southern Part of Ethiopia.

The Linsser filtering of the Bouguer anomalies was applied to delineate vertical and sub-vertical density boundaries. Calculation of Linsser indications was done on a square grid of complete Bouguer anomalies with a 500 m spacing (Figure 24) using the currently developed MATLAB code following the procedure described by Šefara (Šefara, 1973; Šefara and Obr, 1973). The indications were computed for several depth layers (0.5, 1, 2, 4 and 8 km), the length of the Linsser operator increased from 5 km for the 500 m depth to 80 km for the depth of 8 km. The largest depth (8 km) did not yield any useful result for such small region and therefore in the following text this depth level is omitted.

The Linsser indications show density differences which are in some cases related to fault zones. The positions of density contacts at depths of 0.5, 1, 2 and 4 km were plotted in Figure 25. If a fault (contact) dips exactly vertically, all symbols of the Linsser indications plot on top of each other. Slight offsets indicate the fault dip and its direction among the depth levels 0.5, 1, 2 and 4 km.

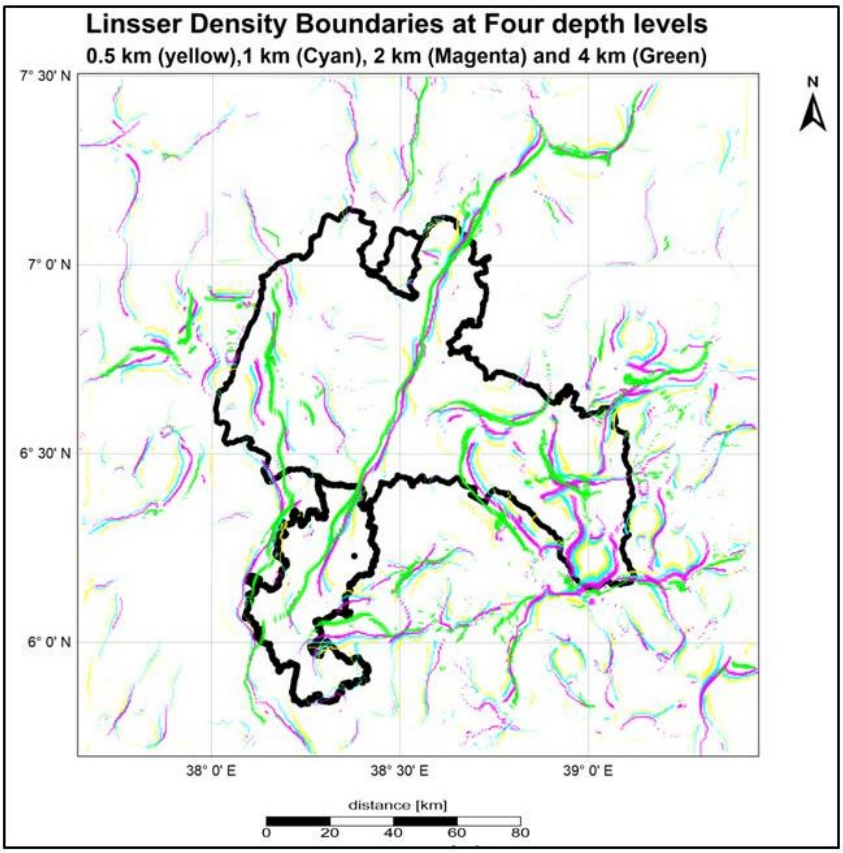

Figure 25: Linsser density boundaries at four depth levels; 0.5 (yellow) 1 km (cyan), 2 km (magenta) and 4 km (green)

The 0.5 km and 1 Km Linsser indications define the near-surface features (Figure 26), whereas 2 and 4 Km Linsser indications define the deeper fault systems (Figure 27).

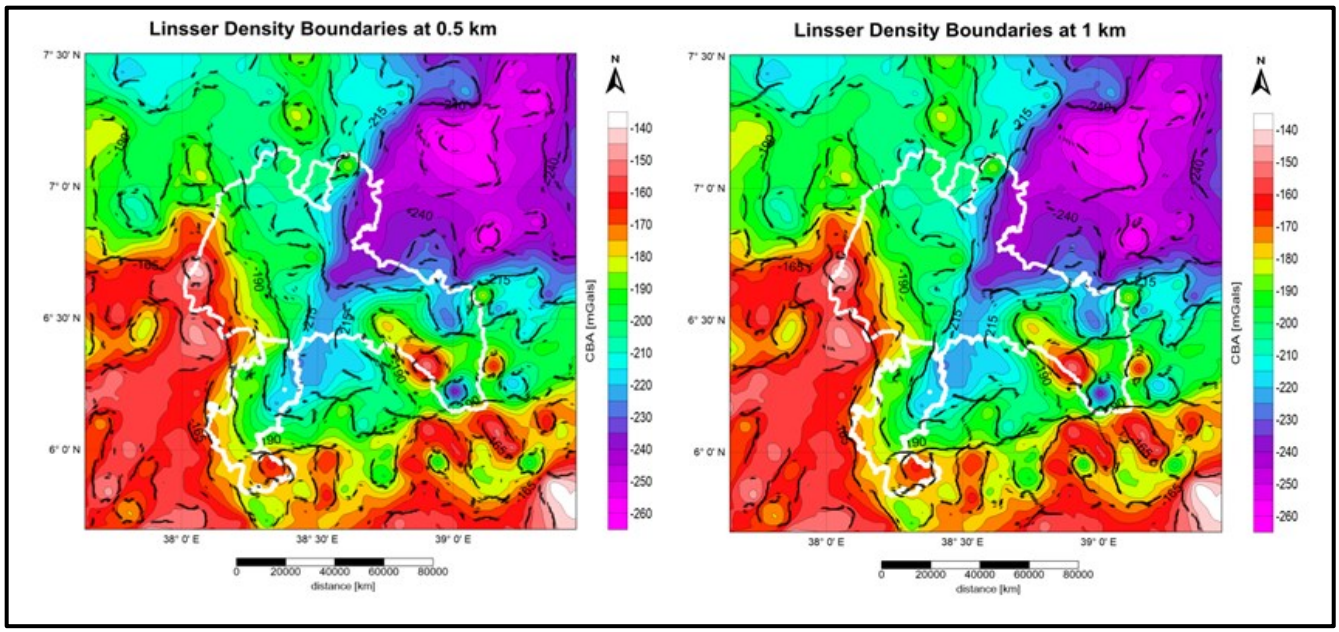

Figure 26: Airborn Bouguer anomaly map of Sidama and Gedeo overlaid by Linsser anomaly map at depth level of 0.5 and 1 Km.

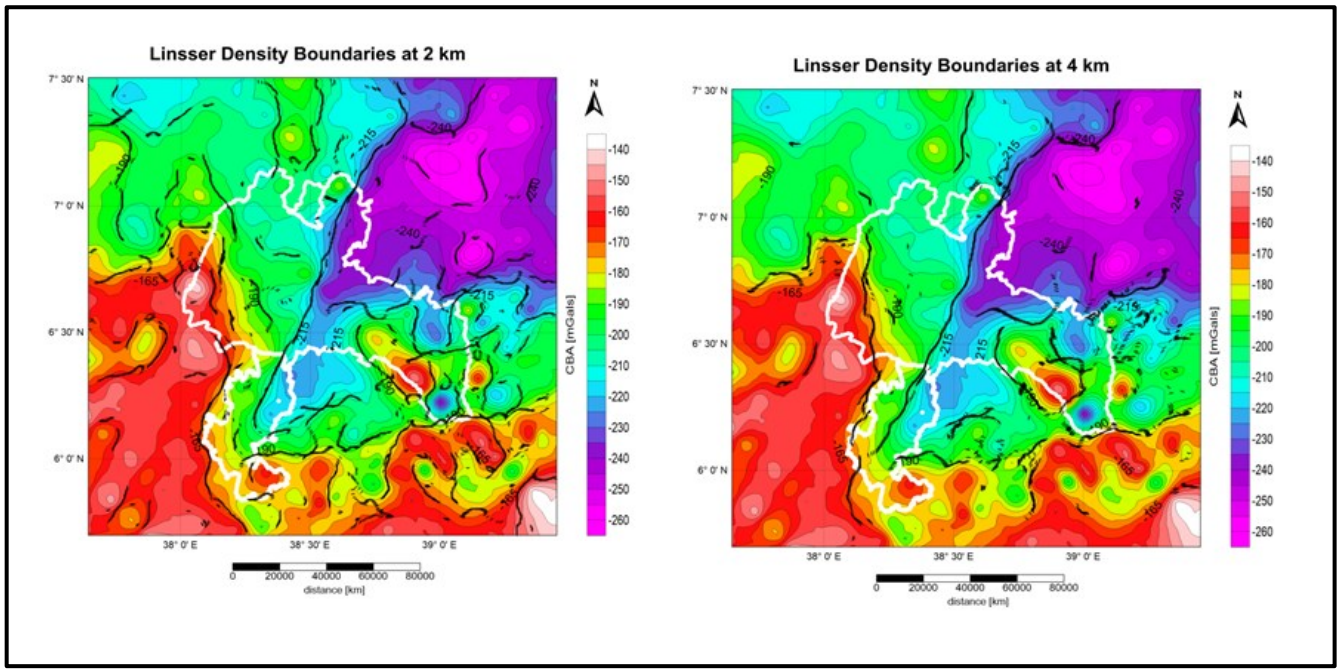

Figure 27: Airborne Bouguer anomaly map of the Sidama and Gedeo zones overlaid by Linsser anomaly map at depth level of 2 and 4 Km.

The interpretation of depth levels at 0.5, 1, 2, and 4 km reveals two sets of faults. These fault sets are distinguished by their colors: the regional faults are marked in red, and the minor faults are marked in blue (Figure 28). The regional faults exhibit directions of NS, NE-SW, and EW, while the minor faults show directions of NS, NE-SW, EW, and NW-SE (Figure 28).

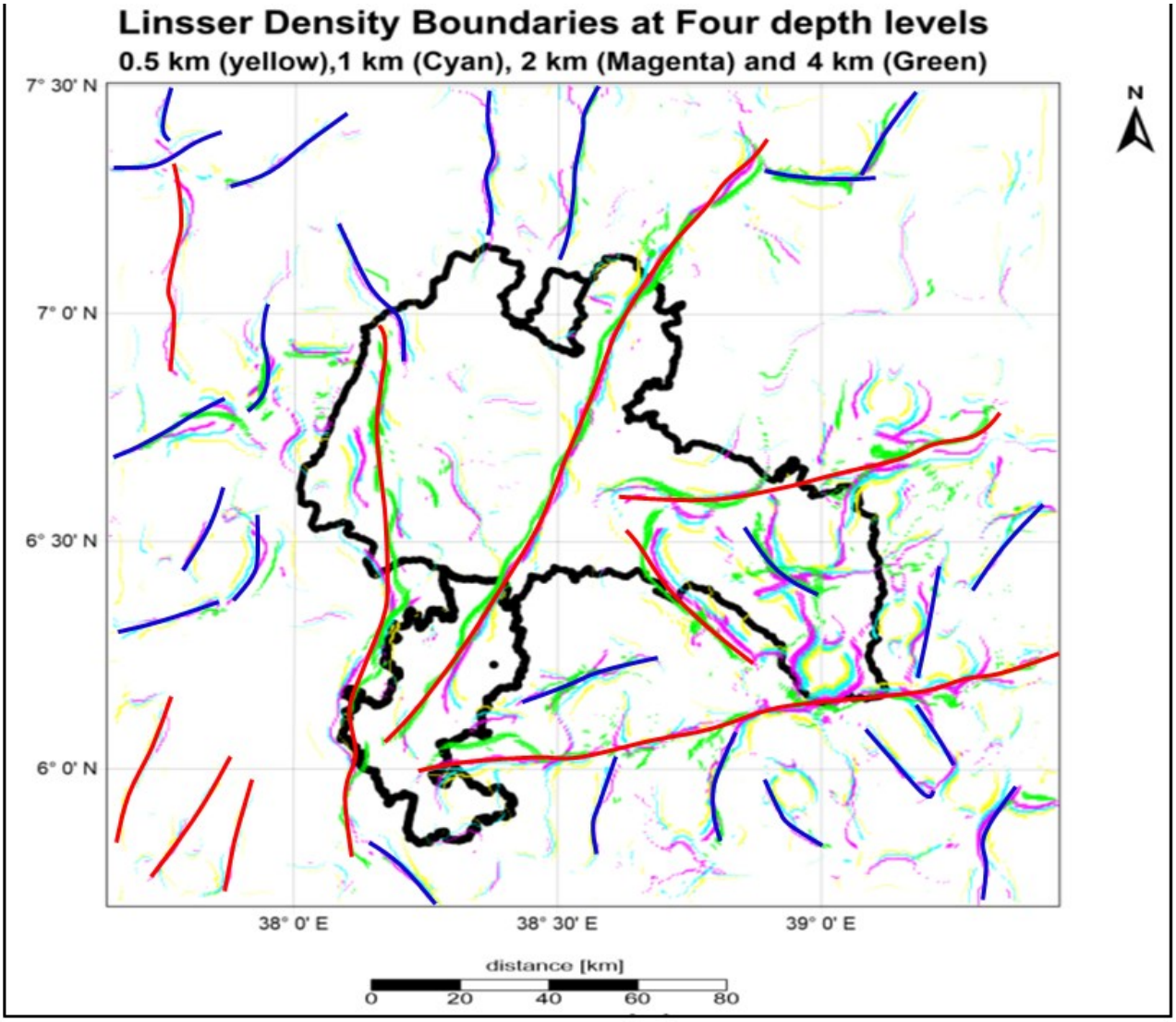

Figure 28: Interpretation of the Linsser anomaly in depth intervals of 0.5, 1, 2, and 4 km reveals distinct fault patterns. Regional faults are depicted in red, while minor faults are represented in blue.

4.3.5 Gedeo Region

The Gedeo area is situated on the south-east margin of the Southern Main Ethiopian Rift. Different segments of the Main Ethiopian Rift represent various stages of E-W continental extension between the Nubian and Somalian plates. In Figure 29, the tectonic map of the Gedeo area, along with the Linsser indication at 0.5 km depth, shows a remarkable similarity in fault orientation.

This shallow indication at 0.5 km depth could be attributed to late rift activity during the Pleistocene age. On the other hand, at depths of 1, 2 and 4 km, the presence of rifting is also evident within the Gedeo area. These deeper indications are most likely associated with the continental extension that commenced during the early rifting phase in the Southern Main Ethiopian Rift during the Lower Miocene period (SOURCE).

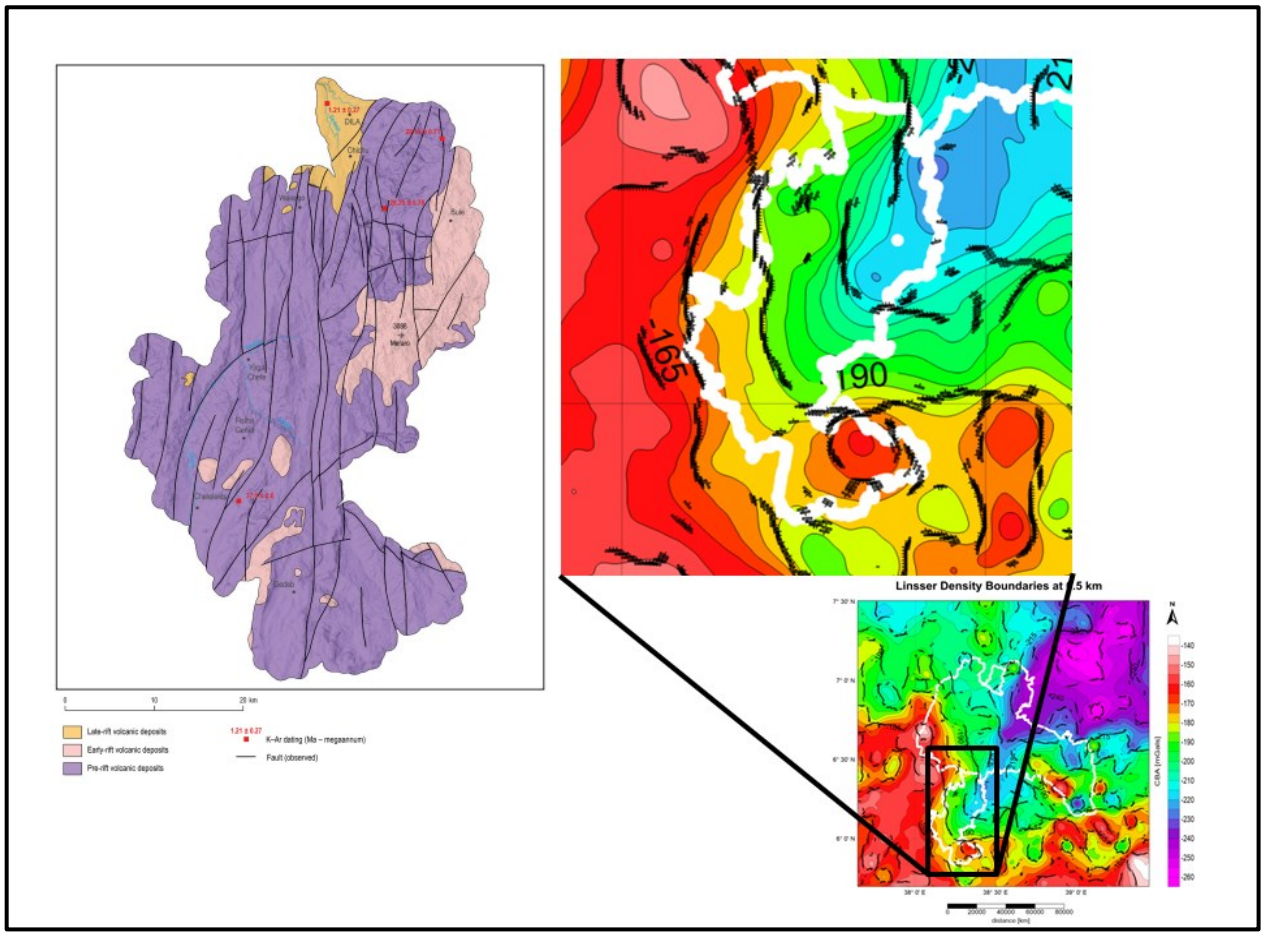

Figure 29: Tectonic map of the Gedeo area and Linsser anomaly of 0.5 km depth superimposed on the Bouguer Gravity anomaly map.

In Figure 20, prominent features include NS (North-South) and NE-SW (Northeast-Southwest) striking faults. These faults are on a regional scale and can be clearly identified by the Linsser depth levels at 1, 2 and4 km.

On a regional scale, the initial extension direction, which was WNW-ESE (West-Northwest to East-Southeast), has undergone recent changes to a W-E (West to East) direction (Agostini et al., 2011). The apparent reactivation of earlier normal faults has resulted in changes in the orientation of the regional stress field, shifting from rift-perpendicular extension to approximately WSW-ESE (West-Southwest to East-Southeast) transtension (Agostini et al., 2011). The main deformation affecting the Gedeo area occurred during the Pliocene to Pleistocene epochs (Rapprich et al., 2014).

The main structures indicated by density contrasts has a NS and NE-SW direction in the geological formations (basalt and trachybasalt lavas) are mainly related to the young rifts of Pliocene to Pleistocene, whereas the more chaotic indications on the SE of the area indicate older (Eocene) stratigraphic sequences (linked to continental extension of early rifting which took place during lower Miocene times) and Precambrian crystalline basement hidden below the younger Tertiary basalts. This means that with the help of Linsser indications one can approximately identify the positions of units up to several depths.

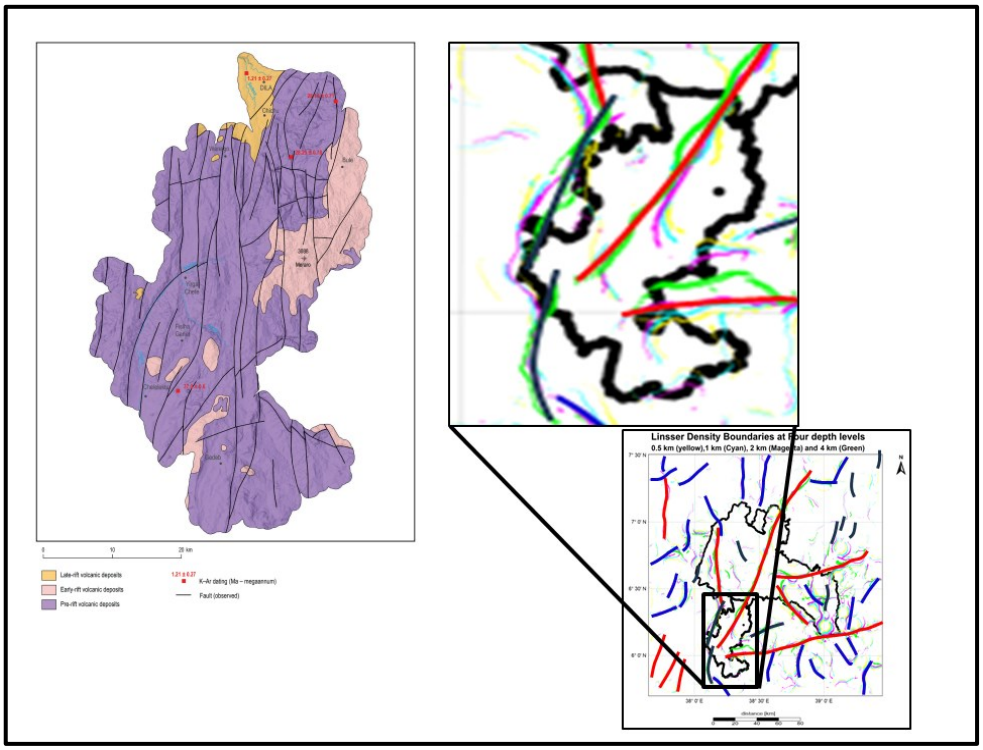

Figure 30: Tectonic map of the Gedeo area and fault interpretation of Linsser anomaly map of 0.5, 1, 2, and 4 km depth

4.3.6 Linsser Anomaly of Sidama Region

The Sidama Region is situated in the southern part of the NNE–SSW trending Southern Main Ethiopian Rift as a part of the East African Rift. Different segments of the Main Ethiopian Rift represent various stages of E-W continental extension between the Nubian and Somalian plates. In Figure 33, the tectonic map of the Sidama area, along with the Linsser indication at 0.5 km and 1 km depth, shows a remarkable similarity in fault orientation.

This shallow indication at 0.5 km depth is primarily attributed to late rift activity during the Eocene to Oligocene ages, whereas the deeper indications related to 1, 2 and 4 Km depth are associated with the continental extension that commenced during the early rifting phase in the Southern Main Ethiopian Rift during the Lower Miocene period (Chorowicz et al., 1994; Acocella and Korme, 2002; Gani et al., 2009).

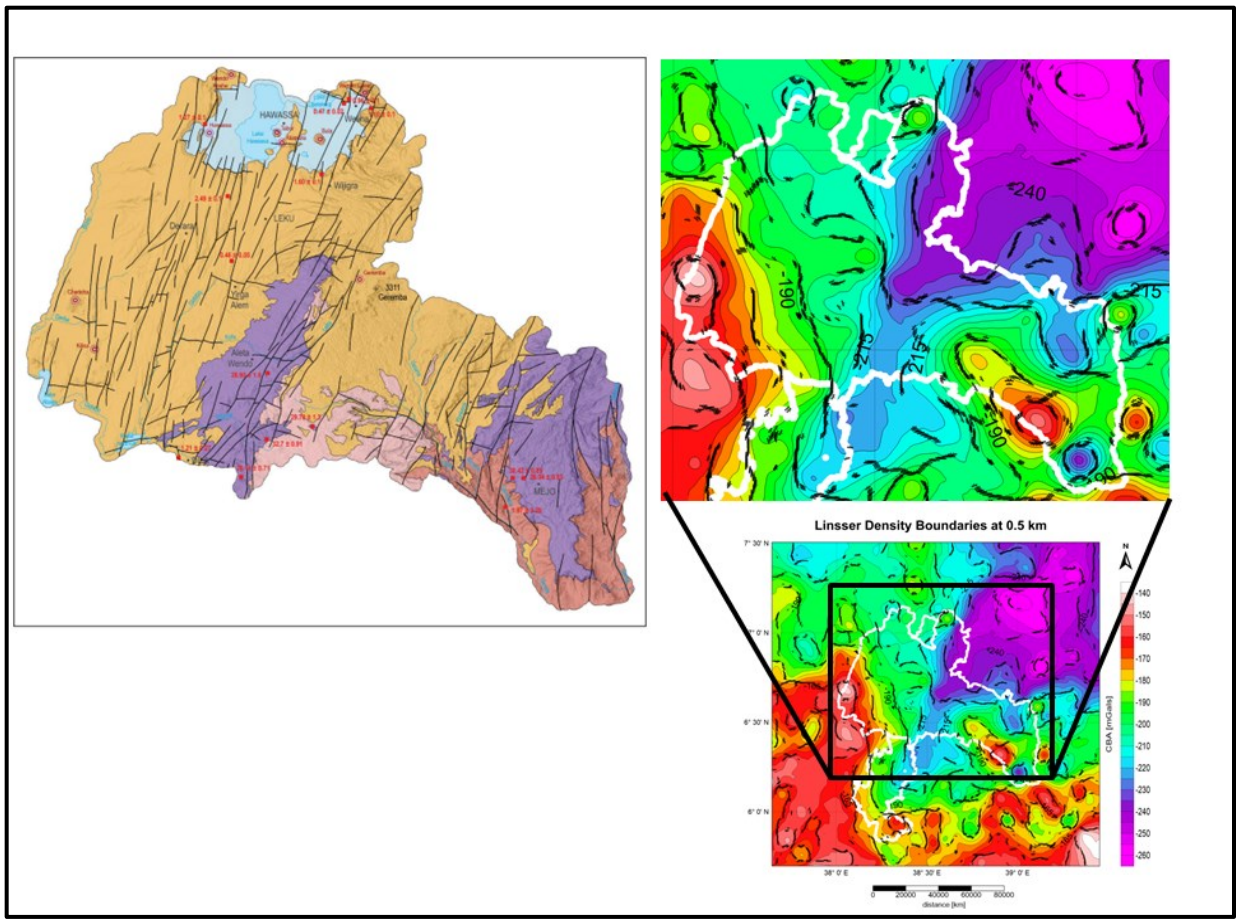

Figure 31: Tectonic map of the Sidama area and Linsser anomaly map of 0.5 km depth superimposed on the Bouguer Gravity anomaly map.

The Sidama area's geological structure is greatly impacted by regional faults and fault zones associated with the Main Ethiopian Rift, which are primarily parallel to the rift's NNE(N)–SSW(S) oriented axis. Most of these faults are vertical and trend NNE-SSW, N-S, or WNW-ESE, and the set of normal faults has a E–W trend (Figure 32). Furthermore, subordinate shear joints or minor faults were mapped for minor oblique-to-strike-slip faults that had both left- and right-lateral kinematic indicators.

The main structures indicated by density contrasts has a N-S and NE-SW direction and are mainly related to the young rifts basalts and trachybasalts of the Pleistocene to Holocene, whereas the more chaotic indications on the SE of the area indicate older (Precambrian) units hidden below the Tertiary basalts. (The basalts might be linked to continental extension of early rifting which took place during Eocene to Oligocene times). This means that with the help of Linsser indications one can approximately identify the stratigraphic units for several depths.

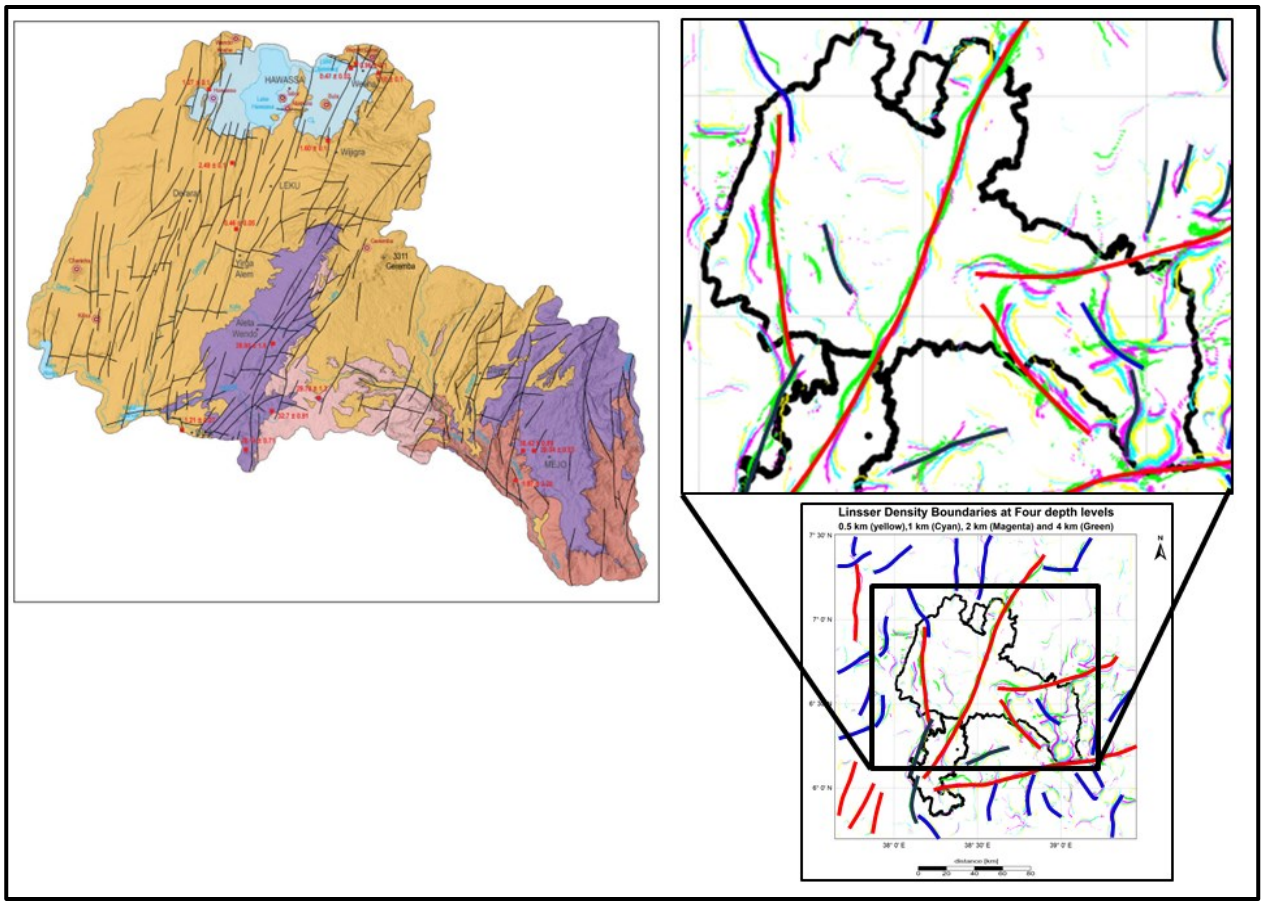

Figure 32: Tectonic map of the Sidama area and fault interpretation of Linsser anomaly map of 0.5, 1, 2, and 4 km depth

5 Discussion

The northernmost part of the East African Rift System (EARS) is the Ethiopian Rift, connecting with the Red Sea and Gulf of Aden rifts. The Main Ethiopian Rift (MER) is the one segment of The Ethiopian Rift, which is a narrow valley separating the Nubian and Somalian plates (Rogers, 2006; Wolfenden et al., 2004). The rift formed through the southward propagation of the Red Sea rift and the northward migration of the EARS (Tommasini et al., 2005). Over time, the MER deepened and widened through a series of overlapping half-graben segments and is divided into three segments: the northern, central, and southern (Corti, 2009; Tesfaye et al., 2003). The central segment − the Afar Depression − acts as a triple junction where the Gulf of Aden, the Red Sea, and the Main Ethiopian Rift converge. The depression is divided into northern, central, and southern sectors based on its physiography and tectonic divisions.

Ethiopia's gravity field shows that the MER and, especially, the northern Afar have regional gravity maxima indicating crustal thinning. The southern Afar, compared to the north one, may contain larger portion of a continental crust due to slightly decreased values of Bouguer anomalies, which is in a good agreement with research of (Kassa et al., 2021) The main rift has a zone of crustal thinning (31 km) with intrusions in the upper crust. The crust thickness is around 50 km on the southeast and northwest sides (Kassa et al., 2021; Mahatsente et al., 2000). Moho depth decreases from central to northern MER. The Bouguer Anomaly map categorizes Ethiopia into four regions based on gravity anomalies: MER with a regional gravity maximum, southern Ethiopian rift with increasing anomalies towards the south, eastern Ethiopian plateau with lower anomalies, and western Ethiopian plateau with the highest anomalies. The Afar depression displays increasing values of the CBA from the MER towards the north. Gravity field of the Main Ethiopian Rift (MER) suggests that the crust beneath the central MER is thicker compared to the southern Afar region.

The Afar depression itself stands out from the CBA map as a distinct area of a regional gravity maximum. The values of CBA reach here values almost 0 mGal (Figure 19), which are the highest values of the whole Ethiopian territory. This gravity high is connected with a very thin crust and shallow depth to the higher-density mantle. Increased values of CBA reflect shallowing of the MOHO depth up to approximately 30 km in the southern part of the Depression (calculated by Kassa et al. (2021) from the gravity data). Increased CBA values further north suggest additional thinning of the crust which is in a good agreement with findings of Kumar et al. (2021) who calculated from receiver functions that the crust thickness reduces to 20 km. The nature of the newly created crust here is still under discussion. Although it could be expected that the newly created crust would be oceanic, Mohr (1989) and Kumar et al. (2021) found evidence of both − continental

and oceanic − leading them to hypothesis about dual-layering of the Afar crust (Kassa et al., 2021; Kumar et al., 2021; Mohr, 1989).

The study further focuses on the Gedeo and Sidama regions within the Southern Main Ethiopian Rift. In both areas, the Linsser indications at different depths (0.5 km and deeper) show similarities in vertical density interfaces (generally interpreted as faults) orientation. Especially the deeper indications (from 2 and 4 km depth) maps the deep subsurface geology. The long continuous N-S or NE-SW trending indications (Figure 31 and 33) marks the rift-related young geology with a simple structure predominantly consisting of horizontal or only slightly inclined volcanic layers splitted mainly by rift-parallel and rift perpendicular fault zones. In contrast, the more complex pattern of Linsser indications on east and south-east of the surveyed area indicates more complicated geological structures of the old Precambrian units.

Within the rift zone, the Linsser indications maps primarily the margin faults of the rift. Their position is clearly marked especially by the 2 and 4 km depths of indications. Slight lateral shifts in them further indicate inclination of the faults (inclination to east for the western line and opposite inclination for the east margin). Such inclinations are in accordance with geological assumptions (Hinze et al., 2012; Pick et al., 1973)) as well as with geophysical models (Tessema and Antoine, 2004; Kassa et al., 2021; Kebede et al., 2022; Kebede et al., 2023).

The NW-SE trending line of indications running in the middle of the rift sone close to the southern boundary of the Sidama zone has currently no placid geological interpretation and must be investigated further.

The distribution of Linsser indications for individual depths in the east and south-east part of the area (the Precambrian units) suggests that the depth of these rocks below the surface is shallower than previously expected by Verner and Megerssa (Verner et al., 2022) who mapped the thickness of overlying igneous rocks to approximately 1500 m. However, since these structures are reflected also on Linsser indications for the shallowest depth of 500 m the depth to the Precambrian units seems to be much shallower. Alternatively, the Precambrian fault structures could also be “copied” through the overlying younger layers, or both of these hypotheses could be valid simultaneously.

6 Conclusion

The East African Rift System (EARS) is an impressive tectonic phenomenon stretching about 6000 kilometers from Syria to central Mozambique. It actively pulls apart the African plate, creating new plates like the Somalian and Danakil Microplates. The Afar Depression, a crucial part of the EARS, serves as a triple junction where the Gulf of Aden, the Red Sea, and the Main Ethiopian Rift converge. Ethiopia's geology is diverse, with Precambrian rocks in linear belts, Cenozoic volcanic rocks covering much of the land, and sedimentary basins such as the Ogaden Basin, the Abay (Blue Nile) Basin, and the Mekele Basin formed during the Gondwanaland breakup.

Since the 1960s, extensive gravity studies in Ethiopia focused on the Main Ethiopian Rift (MER) and northeastern Afar. They found regional Bouguer gravity maximas in the MER and northern Afar, indicating crustal thinning, while the southern Afar region has less thinning and possibly continental crust. Recent studies provided detailed crustal scale models, identifying thinning and thickening zones in various regions.

The Bouguer gravity anomaly map reveals distinct regions with gravity highs and lows, including a maximum over the Main Ethiopian Rift due to thinning or intrusions. The western plateau has a gravity low, and the eastern plateau exhibits a negative anomaly. The Afar triple junction displays significant positive anomalies aligned with the Ethiopian rift, while the southern Ethiopian rift and Turkana rift have negative gravity anomalies. The increase in the CBA values proves estimates that the crust thickness decreases northward from about 50 km in non-rift areas to approximately 20 km in the Afar region and possibly also supports the hypothetical presence of high-density lower crust.

The Gedeo Zone in southern Ethiopia is part of the active Southern Main Ethiopian Rift, known for its rift-related volcanic and volcaniclastic deposits spanning from the Eocene to the present. The region is divided into three main lithotectonic units: pre-rift, early-rift, and late-rift volcanic deposits, each with distinct characteristics. Additionally, the zone contains Quaternary sediments, providing insights into gravity-driven processes and environmental conditions.

The Sidama Region in southern Ethiopia has a diverse geological setting, including high- to medium-grade metamorphic rocks from the Neoproterozoic Southern Ethiopian Shield, as well as volcanic and volcaniclastic deposits associated with the Southern Main Ethiopian Rift. The region has experienced multiple tectonothermal events and magmatic episodes, leading to the formation of various lithotectonic units. The

volcanic activity in the region can be classified into three major episodes, comprising various volcanic and volcaniclastic rocks such as lava flows, ignimbrites, and pyroclastic deposits. The Sidama Region's stratigraphy is well-defined, covering a range of lithological units from the oldest Neoproterozoic rocks to Quaternary volcanic deposits.

The Linsser filtering technique was applied to gravity data in the Gedeo and Sidama regions, both located within the Southern Main Ethiopian Rift. The filtering process revealed the presence of regional and minor faults at various depths, providing insights into the geological structure of these areas.

In the Gedeo region, shallow indications at 0.5 km depth are attributed to late rift activity during the Pleistocene age, while deeper indications at 1, 2 and 4 km suggest continental extension during the early rifting phase in the Lower Miocene period. Prominent NS and NE-SW striking faults were identified, indicating regional-scale deformation that occurred during the Pliocene to Pleistocene epochs.

In the Sidama region, shallow indications at 0.5 km and 1 km depth are associated with late rift activity during the Eocene to Oligocene ages, while deeper indications suggest continental extension during the early rifting phase in the Lower Miocene period. Regional faults parallel to the NNE-N-SSW-S axis of the rift were observed, along with a subordinate set of E-W trending normal faults and minor oblique- to strike-slip faults.

References:

Acocella, V., 2010. Coupling volcanism and tectonics along divergent plate boundaries: Collapsed rifts from central Afar, Ethiopia. Geological Society of America Bulletin 122, 1717–1728. https://doi.org/10.1130/B30105.1

Agostini, A., Bonini, M., Corti, G., Sani, F., Manetti, P., 2011. Distribution of Quaternary deformation in the central Main Ethiopian Rift, East Africa: DEFORMATION IN THE MAIN ETHIOPIAN RIFT. Tectonics 30, n/a-n/a. https://doi.org/10.1029/2010TC002833

Alden, A., 2020. Densities of common rocks and minerals. ThoughtCo.

Amarante, R.R., Trabanco, J.L.A., 2016. Calculation of the tide correction used in gravimetry. Brazilian Journal of Geophysics 34, 193–206.

Anderson, A.J., Cazenave, A., 1986. Space geodesy and geodynamics. London and San Diego.

Barrat, J.A., Fourcade, S., Jahn, B.M., Cheminée, J.L., Capdevila, R., 1998. Isotope (Sr, Nd, Pb, O) and trace-element geochemistry of volcanics from the Erta'Ale range (Ethiopia). Journal of Volcanology and Geothermal Research 80, 85–100. https://doi.org/10.1016/S0377-0273(97)00016-4

Beyene, A., Abdelsalam, M.G., 2005. Tectonics of the Afar Depression: A review and synthesis. Journal of African Earth Sciences 41, 41–59. https://doi.org/10.1016/j.jafrearsci.2005.03.003

Bielik, M., Kovac, M., Kučera, I., Michalík, P., Šujan, M., Hók, J., 2002. Neo-Alpine linear density boundaries (faults) detected by gravimetry. Geologica Carpathica 53, 235–244.

Bonini, M., Corti, G., Innocenti, F., Manetti, P., Mazzarini, F., Abebe, T., Pecskay, Z., 2005. Evolution of the Main Ethiopian Rift in the frame of Afar and Kenya rifts propagation. Tectonics 24, n/a-n/a. https://doi.org/10.1029/2004TC001680

Boone, S.C., Balestrieri, M. -L., Kohn, B.P., Corti, G., Gleadow, A.J.W., Seiler, C., 2019. Tectonothermal Evolution of the Broadly Rifted Zone, Ethiopian Rift. Tectonics 38, 1070–1100. https://doi.org/10.1029/2018TC005210

Buriánek, D, Martínek, K., Šíma, J., Janderková, J., Verner, K., Megerssa, L., Hroch, T., Pacherová, P., Getie, B., Samuel, G., Melaku, A., Jelének, J., Tadege, A., Niguse, B., Tarekegn, D., Hejtmánková, P., Laštovička, J., Bezuneh, M., Dvořák, Š., Štych, P., Melese, T., Valenta, J., Čermáková, D., Zelenková, K., Hrabalíková, M., Ureš, J., Valchářová, D., Spálovský, V., Tsehay, A., Muhuddin, A., Yonas, W., Nol, O., Vaverka, L., 2022. Geology, Soil Environment and Hydrogeology of the Gedeo Zone, Ethiopia. Explanatory notes to the thematic geoscientific maps at a 1 : 100,000 scale. Czech Geological Survey, Prague, Czech Republic.

Carbone, D., Antoni-Micollier, L., Hammond, G., De Zeeuw - Van Dalfsen, E., Rivalta, E., Bonadonna, C., Messina, A., Lautier-Gaud, J., Toland, K., Koymans, M., Anastasiou, K., Bramsiepe, S., Cannavò, F., Contrafatto, D., Frischknecht, C., Greco, F., Marocco, G., Middlemiss, R., Ménoret, V., Noack, A., Passarelli, L., Paul, D., Prasad, A., Siligato, G., Vermeulen, P., 2020. The NEWTON-g Gravity Imager: Toward New Paradigms for Terrain Gravimetry. Front. Earth Sci. 8, 573396. https://doi.org/10.3389/feart.2020.573396

Chorowicz, J., 2005. The East African rift system. Journal of African Earth Sciences 43, 379–410. https://doi.org/10.1016/j.jafrearsci.2005.07.019

Collet, B., Taud, H., Parrot, J.F., Bonavia, F., Chorowicz, J., 2000. A new kinematic approach for the Danakil block using a Digital Elevation Model representation. Tectonophysics 316, 343–357. https://doi.org/10.1016/S0040-1951(99)00263-2

Corti, G., 2009. Continental rift evolution: From rift initiation to incipient break-up in the Main Ethiopian Rift, East Africa. Earth-Science Reviews 96, 1–53. https://doi.org/10.1016/j.earscirev.2009.06.005

Ebinger, C.J., Bechtel, T.D., Forsyth, D.W., Bowin, C.O., 1989. Effective elastic plate thickness beneath the East African and Afar plateaus and dynamic compensation of the uplifts. J. Geophys. Res. 94, 2883–2901. https://doi.org/10.1029/JB094iB03p02883

Ebinger, C.J., Casey, M., 2001. Continental breakup in magmatic provinces: An Ethiopian example. Geol 29, 527. https://doi.org/10.1130/0091-7613(2001)029<0527:CBIMPA>2.0.CO;2
Ebinger, C.J., Hayward, N.J., 1996. Soft plates and hot spots: Views from Afar. J. Geophys. Res. 101, 21859–21876. https://doi.org/10.1029/96JB02118
Ebinger, C.J., Ibrahim, A., 1994. Multiple episodes of rifting in Central and East Africa: A re-evaluation of gravity data. Geol Rundsch 83. https://doi.org/10.1007/BF00251068
Ebinger, C.J., Yemane, T., Harding, D.J., Tesfaye, S., Kelley, S., Rex, D.C., 2000. Rift deflection, migration, and propagation: Linkage of the Ethiopian and Eastern rifts, Africa. Geological Society of America Bulletin 112, 163–176. https://doi.org/10.1130/0016-7606(2000)112<163:RDMAPL>2.0.CO;2
Ebinger, C.J., Yemane, T., Woldegabriel, G., Aronson, J.L., Walter, R.C., 1993. Late Eocene–Recent volcanism and faulting in the southern main Ethiopian rift. JGS 150, 99–108. https://doi.org/10.1144/gsjgs.150.1.0099
EROS, U., 2018. Digital Elevation-Shuttle Radar Topography Mission (SRTM) 1 Arc-Second Global. Erişim Adresi: https://earthexplorer. usgs. gov.
Fairhead, J.D., Odegard, M.E., 2002. Advances in gravity survey resolution. The Leading Edge 21, 36–37. https://doi.org/10.1190/1.1445845
Fritz, H., Abdelsalam, M., Ali, K.A., Bingen, B., Collins, A.S., Fowler, A.R., Ghebreab, W., Hauzenberger, C.A., Johnson, P.R., Kusky, T.M., Macey, P., Muhongo, S., Stern, R.J., Viola, G., 2013. Orogen styles in the East African Orogen: A review of the Neoproterozoic to Cambrian tectonic evolution. Journal of African Earth Sciences 86, 65–106. https://doi.org/10.1016/j.jafrearsci.2013.06.004
Gadirov, V., Kalkan, E., Ozdemir, A., Palabiyik, Y., Gadirov, K., 2022. Use of gravity and magnetic methods in oil and gas exploration: Case studies from Azerbaijan. International Journal of Earth Sciences Knowledge and Applications 4, 143–156.
Gani, N.Ds., Abdelsalam, M.G., Gera, S., Gani, M.R., 2009. Stratigraphic and structural evolution of the Blue Nile Basin, Northwestern Ethiopian Plateau. Geol. J. 44, 30–56. https://doi.org/10.1002/gj.1127
George, R., Rogers, N., 2002. Plume dynamics beneath the African plate inferred from the geochemistry of the Tertiary basalts of southern Ethiopia. Contrib Mineral Petrol 144, 286–304. https://doi.org/10.1007/s00410-002-0396-z
Ghebreab, W., 1992. The geological evolution of the Adola Precambrian greenstone belt, Southern Ethiopia. Journal of African Earth Sciences (and the Middle East) 14, 457–469. https://doi.org/10.1016/0899-5362(92)90078-Q
Griffiths, D.H., King, R.F., 2013. Applied geophysics for geologists and engineers: the elements of geophysical prospecting. Elsevier.
Hammer, S., 1939. Terrain corrections for gravimeter stations. GEOPHYSICS 4, 184–194. https://doi.org/10.1190/1.1440495
Hatch, R.R., 2007. A new theory of Gravity: overcoming problems with general relativity. Physics Essays 20, 83–100.
Hendrie, D.B., Kusznir, N.J., Morley, C.K., Ebinger, C.J., 1994. Cenozoic extension in northern Kenya: a quantitative model of rift basin development in the Turkana region. Tectonophysics 236, 409–438. https://doi.org/10.1016/0040-1951(94)90187-2
Hill, P., Bankey, V., Langenheim, V., 1997. Introduction to Potential Fields: Gravity (Fact Sheet No. 239–95), USGS Numbered Series.
Hinze, W.J., Von Frese, R.R.B., Saad, A.H., 2012. Gravity and Magnetic Exploration: Principles, Practices, and Applications, 1st ed. Cambridge University Press. https://doi.org/10.1017/CBO9780511843129
Jäggi, A., Bock, H., Prange, L., Meyer, U., Beutler, G., 2011. GPS-only gravity field recovery with GOCE, CHAMP, and GRACE. Advances in Space Research 47, 1020–1028. https://doi.org/10.1016/j.asr.2010.11.008
Jentzsch, G., Mahatsente, R., Jahr, T., 2000. Three dimensional inversion of gravity data from the main ethiopian Rift. Physics and Chemistry of the Earth, Part A: Solid Earth and Geodesy 25, 365–373.

https://doi.org/10.1016/S1464-1895(00)00058-2
Kassa, M., Alemu, A., Muluneh, A., 2021. Determination of gravity and isostatic Moho: Implications for the evolution of rifting in the central Main Ethiopian Rift. Journal of African Earth Sciences 184, 104350. https://doi.org/10.1016/j.jafrearsci.2021.104350
Kumar, U., Legendre, C.P., Huang, B.S., 2021. Crustal structure and upper mantle anisotropy of the Afar triple junction. Earth Planets Space 73, 166. https://doi.org/10.1186/s40623-021-01495-0
LaFehr, T.R., 1991. Standardization in gravity reduction. GEOPHYSICS 56, 1170–1178. https://doi.org/10.1190/1.1443137
Linsser, H., 1967a. Ivestigation of Tectonics by Gravity detailing. Geophysical Prospecting 15, 480–515.
Linsser, H., 1967b. NVESTIGATION OF TECTONICS BY GRAVITY DETAILING*. Geophysical Prospecting 15, 480–515. https://doi.org/10.1111/j.1365-2478.1967.tb01800.x
Loj, M., Porzucek, S., 2019. Detailed analysis of the gravitational effects caused by the buildings in microgravity survey. Acta Geophysica 67, 1799–1807.
Mahatsente, R., Jentzsch, G., Jahr, T., 2000. Three-dimensional inversion of gravity data from the Main Ethiopian Rift. Journal of African Earth Sciences 31, 451–466. https://doi.org/10.1016/S0899-5362(00)00099-3
Makris, J., Menzel, H., Zimmermann, J., 1972. A Preliminary Interpretation of the Gravity Field of Afar, Northeast Ethiopia, in: Developments in Geotectonics. Elsevier, pp. 31–39. https://doi.org/10.1016/B978-0-444-41087-0.50008-7
Mareš, S., 1990. Úvod do užité geofyziky: celost. vysokošk. učebnice pro stud. přírodověd. fakult, 2., přeprac. vyd. ed. SNTL, Praha.
Mickus, K., 2003. Gravity method: environmental and engineering applications. Presented at the Department of Geosciences, Southwest Missouri State University, Springfield http://www. dot. state. fl. us/statematerialsoffice/Geotechnical/conference/materials/mickus. pdf Search in.
Mickus, K., Tadesse, K., Keller, G.R., Oluma, B., 2007. Gravity analysis of the main Ethiopian rift. Journal of African Earth Sciences 48, 59–69. https://doi.org/10.1016/j.jafrearsci.2007.02.008
Mickus, K.L., Hinojosa, J.H., 2001. The complete gravity gradient tensor derived from the vertical component of gravity: a Fourier transform technique. Journal of Applied Geophysics 46, 159–174. https://doi.org/10.1016/S0926-9851(01)00031-3
Minissale, A., Corti, G., Tassi, F., Darrah, T.H., Vaselli, O., Montanari, D., Montegrossi, G., Yirgu, G., Selmo, E., Teclu, A., 2017. Geothermal potential and origin of natural thermal fluids in the northern Lake Abaya area, Main Ethiopian Rift, East Africa. Journal of Volcanology and Geothermal Research 336, 1–18. https://doi.org/10.1016/j.jvolgeores.2017.01.012
Mohr, P., 1989. Nature of the crust under Afar: new igneous, not thinned continental. Tectonophysics 167, 1–11. https://doi.org/10.1016/0040-1951(89)90290-4
Mohr, P., Rogers, A., 1966. Gravity traverses in Ethiopia: Bulletin of the Geophysical Observatory. Haile Selassie I University 9, 7–58.
Mulugeta, B.D., Fujimitsu, Y., Nishijima, J., Saibi, H., 2021. Interpretation of gravity data to delineate the subsurface structures and reservoir geometry of the Aluto–Langano geothermal field, Ethiopia. Geothermics 94, 102093. https://doi.org/10.1016/j.geothermics.2021.102093
Murata Y., Noro H., 1994. Effective imaging of the gravity data using topographic and geological data, Geological Survey Japan 280. ed.
Murray, A., 1997. The Australian national gravity database. AGSO Journal of Australian Geology and Geophysics 17, 145–155.
Nettleton, L.L., 1971. Elementary gravity and magnetics for geologists and seismologists. Society of Exploration Geophysicists.
Nigussie, W., Mickus, K., Keir, D., Alemu, A., Muhabaw, Y., Muluneh, A.A., Yehualaw, E., Demissie, Z., 2023. Subsurface structure of magmatic segments during continental breakup: Perspectives from a gravity data analysis along the Main Ethiopian Rift. Front. Earth Sci. 10, 1092759.

https://doi.org/10.3389/feart.2022.1092759
Philippon, M., Corti, G., Sani, F., Bonini, M., Balestrieri, M.-L., Molin, P., Willingshofer, E., Sokoutis, D., Cloetingh, S., 2014. Evolution, distribution, and characteristics of rifting in southern Ethiopia: rifting in southern Ethiopia. Tectonics 33, 485–508. https://doi.org/10.1002/2013TC003430
Pick, M., Picha, J., Vyskocil, V., 1973. Theory of the earth's gravity field. Amsterdam; New York: Elsevier Scientific Pub. Co.
Rogers, N.W., 2006. Basaltic magmatism and the geodynamics of the East African Rift System. SP 259, 77–93. https://doi.org/10.1144/GSL.SP.2006.259.01.08
Saibi, H., 2018. Microgravity and its applications in geosciences. gravity book, Intech edition 41–72.
Saibi, H., Aboud, E., Ehara, S., 2012. Analysis and interpretation of gravity data from the Aluto-Langano geothermal field of Ethiopia. Acta Geophysica 60, 318–336.
Šefara, J., 1973. Interpretation of vertical densitz interfaces using a map of gravity animalies by means of a digital computer.
Tadesse, S., Milesi, J.-P., Deschamps, Y., 2003. Geology and mineral potential of Ethiopia: a note on geology and mineral map of Ethiopia. Journal of African Earth Sciences 36, 273–313. https://doi.org/10.1016/S0899-5362(03)00048-4
Tang, S., Liu, H., Yan, S., Xu, X., Wu, W., Fan, J., Liu, J., Hu, C., Tu, L., 2019. A high-sensitivity MEMS gravimeter with a large dynamic range. Microsystems & nanoengineering 5, 45.
Tanner, J., Gibb, R., 1979. Gravity method applied to base metal exploration. Geophysics and Geochemistry in the search for metallic ores. Geological Survey of Canada, Economic Geology Report 31, 105–122.
Tefera, M, Cherenet, T., Haro, W, 1996. Geological map of Ethiopia (1:2, 000, 000).
Tesfaye, S., Harding, D.J., Kusky, T.M., 2003. Early continental breakup boundary and migration of the Afar triple junction, Ethiopia. Geo. Society Am. Bull. 115, 1053. https://doi.org/10.1130/B25149.1
Thiessen, R., Burke, K., Kidd, W.S.F., 1979. African hotspots and their relation to the underlying mantle. Geol 7, 263. https://doi.org/10.1130/0091-7613(1979)7<263:AHATRT>2.0.CO;2
Tiberi, C., Ebinger, C., Ballu, V., Stuart, G., Oluma, B., 2005. Inverse models of gravity data from the Red Sea-Aden-East African rifts triple junction zone. Geophysical Journal International 163, 775–787. https://doi.org/10.1111/j.1365-246X.2005.02736.x
Tommasini, S., Manetti, P., Innocenti, F., Abebe, T., Sintoni, M., Conticelli, S., 2005. The Ethiopian subcontinental mantle domains: geochemical evidence from Cenozoic mafic lavas. Mineralogy and Petrology 84, 259–281. https://doi.org/10.1007/s00710-005-0081-9
Verner, K., Buriánek, D., Svojtka, M., Peřestý, V., Megerssa, L., Tadesse, T., Kussita, A., Alemayehu, D., Hroch, T., 2021. Tectonometamorphic evolution and U–Pb dating of the high-grade Hammar Domain (Southern Ethiopian Shield); implications for the East-African Orogeny. Precambrian Research 361, 106270. https://doi.org/10.1016/j.precamres.2021.106270
Verner, K., Megerssa, L.Šíma, J. Buriánek, D. Hroch, T. Dvořák, Š. Martínek, K. Pacherová, P. Basalifew, Z. Negessa, G. Bezuneh, M. Getie, B. Samuel, G. Valenta, J. Jelének, J. Hejtmánková, P. Štych, P. Lastovička, J. Valchářová, D. Čermáková, D. Tsehay, A. Muhuddin, A. Yonas, W. Abebe, M. Melese, T. Belay, M. Niguse, B. Adualem, T. Tarekegn, D. Tadege, A. Abadi, H. Spálovský, V. Nol, O. Vaverka, L. Zelenková, K. Hrabalíková, M. Ureš, 2022. Geology, Soil Environment and Hydrogeology of the Sidama Region, Ethiopia. Geoscience maps. 136 s. –. Czech Geological Survey. Prague, Czech Republic.
Virtanen, H., 2006. Studies of Earth Dynamics with the Superconducting Gravimeter, Academic Dissertation in Geophysics, University of Helsinki.
Visser, P.N.A.M., 1999. Gravity field determination with GOCE and GRACE. Advances in Space Research 23, 771–776. https://doi.org/10.1016/S0273-1177(99)00154-4
Wolfenden, E., Ebinger, C., Yirgu, G., Deino, A., Ayalew, D., 2004. Evolution of the northern Main Ethiopian rift: birth of a triple junction. Earth and Planetary Science Letters 224, 213–228.

https://doi.org/10.1016/j.epsl.2004.04.022
Worku, H., 1996. Tectonic evolution of the Neoproterozoic Adola Belt of southern Ethiopia: evidence for a Wilson Cycle process and implications for oblique plate collision. Precambrian Research 77, 179–210. https://doi.org/10.1016/0301-9268(95)00054-2
Wybraniec, S., 1999. Transformations and visualization of potential field data. Polish Geological Institute Special Papers 1, 1–88.
Yibas, B., Reimold, W.U., Armstrong, R., Koeberl, C., Anhaeusser, C.R., Phillips, D., 2002. The tectonostratigraphy, granitoid geochronology and geological evolution of the Precambrian of southern Ethiopia. Journal of African Earth Sciences 34, 57–84. https://doi.org/10.1016/S0899-5362(01)00099-9
Yihunie, T., Adachi, M., Takeuchi, M., 2004. P-T Conditions of Metamorphism in the Neoproterozoic Rocks of the Negele Area, Southern Ethiopia. Gondwana Research 7, 489–500. https://doi.org/10.1016/S1342-937X(05)70800-5
Zanettin, B., Justin-Visentin, E., 1975. Tectonical and volcanological evolution of the western Afar margin (Ethiopia). E. Schweizerb. Verlag.
Zhang, C., Mushayandebvu, M.F., Reid, A.B., Fairhead, J.D., Odegard, M.E., 2000. Euler deconvolution of gravity tensor gradient data. GEOPHYSICS 65, 512–520. https://doi.org/10.1190/1.1444745
Zhang, J., Zeng, Z., Zhao, X., Li, J., Zhou, Y., Gong, M., 2020. Deep Mineral Exploration of the Jinchuan Cu–Ni Sulfide Deposit Based on Aeromagnetic, Gravity, and CSAMT Methods. Minerals 10, 168. https://doi.org/10.3390/min10020168
Zhang, M., Qiao, J., Zhao, G., Lan, X., 2019. Regional gravity survey and application in oil and gas exploration in China. China Geology 2, 382–390.

Web Sources:

U.S. Geological Survey (2018). USGS EROS Archive - Digital Elevation - Shuttle Radar Topography Mission (SRTM) 1 Arc-Second Global. https://www.usgs.gov/centers/eros/science/usgs-eros-archive-digital-elevation-shuttle-radar-topography-mission-srtm-1?qt-science_center_objects=0#qt-science_center_objects Data downloaded during the year 2021.

Hatch, D. and Pitts,B., 2010. The De Beers airship gravity project. In Lane, R.J.L. (Ed.), Airbourne Gravity 2010 ASEG-PESA Airborne Gravity 2010 Workshop. Geoscience Australia and the Geological Survey of New South Wales, Geoscience. Australia Record 2010/23 and GSNSW File GS2010/0457, 97-106. https://www.yumpu.com/en/document/view/4164325/airborne-gravity-2010-geoscience-australia

List of Figures

List of Abbreviations

ABGD	Airborne Gravity Data
CBA	Complete Bouguer Anomalies
CMER	Central Main Ethiopian Rift
DEM	Digital Elevation Model
DTM	Digital Terrain Models
EA	Erte Ale Region
EARS	East African Rift System
GNSS	Global Navigation Satellite Systems
GOCE	Gravity field and steady-state Ocean Circulation Explorer
GPS	Global Positioning System
GRACE	Gravity Recovery And Climate Experiment
GRS67	Geodetic Reference System, 1967
GSE	Geological Survey of Ethiopia
LiDAR	Light Detection And Ranging
MER	Main Ethiopian Rift
SER	Southern Ethiopian Rift
SMER	Southern Main Ethiopian Rift
SRTM	Shuttle Radar Topography Mission